Shakedown theorems for shape memory alloys structures with functional fatigue - Application to nitinol stents

Michaël Peigney

Shakedown theorems for shape memory alloys structures with functional fatigue – Application to nitinol stents

Michaël Peigney

Lab Navier, Univ Gustave Eiffel, ENPC, CNRS, F-77447 Marne la Vallée, France

Abstract

Shape memory alloys (SMAs) offer interesting perspectives in various fields such as aeronautics, robotics, biomedical sciences, or structural engineering. The distinctive properties of those materials stem from a solid/solid phase transformation occurring at a microscopic level. Modeling the rather complex behavior of SMAs is a topic of active research. Lately, SMA models coupling phase-transformation with permanent inelasticity have been proposed to capture degradation effects which are frequently observed experimentally for cyclic loadings — a phenomenon referred to as functional fatigue. In this paper, the classical static and kinematic shakedown of plasticity theory are extended to such material models. Those results give conditions for the energy dissipation to remain bounded, which is beneficial for the fatigue life. Analytical shakedown limits are obtained for a 3-bar truss example and compared with numerical results from step-by-step simulations. We consider the problem of a nitinol stent submitted to cyclic pressure and mixed pressure–bending as an application, showing how the approach presented can be combined with finite-element analysis to study shakedown of complex 3D structures.

Keywords: Shakedown, Functional fatigue, Shape Memory Alloys, Permanent Inelasticity, Stent

1. Introduction

Shape Memory Alloys (SMAs) display peculiar properties such as the shape memory effect or the superelastic behavior. Those properties result from a solid–solid phase transformation between different crystallographic structures (austenite and

Email address: michael.peigney@polytechnique.org (Michaël Peigney)

martensite). That phase transformation is triggered by thermal or mechanical loading and gives rise to the spontaneous formation of austenite–martensite microstructures at the microscopic scale. Modeling phase transformation SMAs is a complex topic that has received a lot of attention. Various constitutive models have been proposed using phenomenological and/or micromechanical considerations (see e.g. the review by Cisse et al. (2016) as well as the more recent work by Xu et al. (2019); Scalet et al. (2021)). Phase transformation is usually tracked by an internal variable $\boldsymbol{\alpha}_1$ that needs to satisfy some a priori constraints resulting from mass conservation. Such constraints constitute a crucial difference with standard plasticity models and calls for special attention when considering the structural evolution problem (Govindjee and Miehe, 2001; Peigney et al., 2011; Artioli and Bisegna, 2016; Scalet and Peigney, 2017). The peculiar properties of SMAs make them attractive for many applications in domains as varied as aeronautics, civil engineering and biomedicals. A lot of those applications correspond to cyclic loadings, which raises the issue of fatigue. In that regard, one of the most severe cases is nitinol self-expanding stents using in biomedicals for treating artery disease (Duerig et al., 2000; Pelton et al., 2008). Those devices are submitted to pulsatile pressure due to the cardiac cycles. The requirement of fatigue life for stents is extremely high, about 10^8 cycles (Eggeler et al., 2004).

Fatigue of SMAs needs to be subdivided into *structural fatigue* and *functional fatigue* (Eggeler et al., 2004; Antonucci et al., 2021). Structural fatigue corresponds to the accumulation of microscopic damage eventually leading to the initiation and subsequent propagation of cracks. Functional fatigue refers to the decrease of functional properties – such as the maximum recoverable strain (Bhattacharya and Kohn, 1997; Peigney, 2013a,b) – over loading cycles. Structure fatigue is not specific to SMAs and goes back to the pioneering works of the 19th century on metal fatigue (Rankine, 1843; Wohler, 1858; Bauschinger, 1886). The most favorable regime of high-cycle fatigue corresponds to elastic shakedown, i.e. to situations where the total energy dissipation is bounded so that the structures behaves elastically after a sufficiently large number of loading cycles. For elastic-perfectly plastic materials, Melan's theorem (also known as the static shakedown theorem) gives a sufficient condition on the loading for elastic shakedown to occur, independently of any residual stress that may exist in the initial state (Melan, 1936; Koiter, 1960). That theoretical result is complemented by Koiter's theorem (also known as the kinematic shakedown theorem) that gives a necessary condition for shakedown (Koiter, 1960). Combining those two theorems provides bounds on the loadings for which shakedown occurs, thus allowing one to design elastic-perfectly plastic structures against shakedown. Melan's and Koiter's theorems have been extended to several complex behaviors such as nonlin-

ear hardening plasticity (Nguyen, 2003; Pham, 2008, 2017), temperature-dependent material properties (Borino, 2000; Peigney, 2014b), friction coupled with plasticity (Klarbring et al., 2017) or diffusion-induced plasticity (Peigney, 2018, 2020). In particular, a static shakedown theorem applying to SMAs (without any degradation effects) has been proved in Peigney (2014a). For a cyclic loading exceeding the shakedown limit provided by that theorem, the large-time behavior depends on the initial state: some initial conditions lead to shakedown whereas some others lead to alternating phase transformation. Such a feature is not observed in standard plasticity.

By contrast with structural fatigue, functional fatigue is relatively specific to SMAs. For instance, the initiation stress of the austenite to martensite transformation is observed to decrease over consecutive loading cycles. In addition, a permanent strain accumulates in the stress-free state. Several constitutive models have been proposed to capture those effects (Auricchio et al., 2007; Yu et al., 2012; Barrera et al., 2014; Wang et al., 2017; Waimann et al., 2017; Chemisky et al., 2018; Dornelas et al., 2020; Woodworth and Kaliske, 2022). Two internal variables are generally introduced: in addition to the (constrained) variable $\boldsymbol{\alpha}_1$ describing the phase transformation mentioned previously, an internal variable $\boldsymbol{\alpha}_2$ is used to describe permanent inelasticity effects. As discussed notably by Auricchio et al. (2007); Yu et al. (2012), coupling those two variables in the free energy is essential to capture the decrease of initiation stress and the build-up of permanent inelastic strain. This results in a much more complex mathematical structure for the constitutive models.

So far, structural fatigue and functional fatigue have been studied independently from each other. In particular, existing shakedown theorems for SMAs do no take into account the degradation effects of functional fatigue. Over consecutive loading cycles, those degradation effects may cause a redistribution of the stress in the structure which may affect the initiation of fatigue cracks. Structural fatigue and functional fatigue are thus to be considered as coupled phenomena. This paper aims at taking that coupling into account by presenting shakedown theorems for some SMA models of functional fatigue. The class of constitutive models considered is first introduced in Sect. 2 and illustrated with some examples from the literature. The local constitutive laws are combined with equilibrium relations in Sect. 3 to formulate the boundary value problem governing quasi-static evolutions of a continuum from a given initial state when the loading history is prescribed. In Sect. 4 we present a static shakedown theorem giving a sufficient condition on the loading for shakedown to occur whatever the initial state. That theorem leads to the definition of a static safety coefficient with respect to shakedown. The exact evaluation of that coefficient is discussed for two examples of material models. The first example is the model of Auricchio

et al. (2007) which is one of the earliest and most well-known 3D model accounting for functional fatigue. An incremental state update algorithm is available for that model, allowing one to calculate the step-by-step evolution and compare it with predictions of the theorems. The second example is the more recent model of Barrera et al. (2014), which in terms of mathematical structure is quite different from the model of Auricchio et al. (2007). In that case, a reformulation of the model is needed (via a change of variables) for the shakedown theorem to be applied. Using min-max duality, a kinematic shakedown theorem and a corresponding kinematic safety factor are derived in Sect. 5. Those theorems are illustrated on some structural problems in Sects 6 and 7. In Sect. 6 we first consider the simple example of a 3-bar truss. That example (or its closely related 2-bar variant) is frequently used in the field of shakedown theory because the calculation of the shakedown limits can be performed in closed-form (Nguyen, 2003; Feng and Sun, 2007; Hasbroucq et al., 2010; Peigney, 2010). Numerical results from step-by-step simulations are also provided to illustrate the influence of the initial state on the shakedown state. In Sect. 7 we study the more complicated problem of a nitinol stent submitted to cyclic pressure and mixed pressure–bending, showing how the presented approach can be combined with finite-element analysis to study shakedown of complex 3D structures.

2. Constitutive laws

We consider a class of constitutive material models in which the local state of the material is described by the (linearized) strain $\boldsymbol{\varepsilon}$ and two internal variables $(\boldsymbol{\alpha}_1, \boldsymbol{\alpha}_2)$. The variable $\boldsymbol{\alpha}_1$ tracks the phase transformation whereas the variable $\boldsymbol{\alpha}_2$ describes permanent inelasticity effects. To simplify the presentation, we consider the most usual situation where $\boldsymbol{\varepsilon}$ lives in the space $\mathbb{R}_s^{3\times3}$ of symmetric second-order tensors and $\boldsymbol{\alpha}_i$ $(i = 1, 2)$ lives in the space $\mathrm{dev}(\mathbb{R}_s^{3\times3})$ of trace-free symmetric second-order tensors. However, all that follows can directly be extended to situations where $\boldsymbol{\varepsilon}$, $\boldsymbol{\alpha}_2$, $\boldsymbol{\alpha}_1$ live in other spaces than $\mathbb{R}_s^{3\times3}$ and $\mathrm{dev}(\mathbb{R}_s^{3\times3})$.

In the classical framework of generalized standard materials with rate-independent behavior (Halphen and Nguyen, 1975), the constitutive laws are determined by the free energy function $\psi(\boldsymbol{\varepsilon}, \boldsymbol{\alpha}_1, \boldsymbol{\alpha}_2)$ and the elasticity domain $\mathcal{C}$, the latter being a convex subset of $\mathrm{dev}(\mathbb{R}_s^{3\times3}) \times \mathrm{dev}(\mathbb{R}_s^{3\times3})$. In more detail, the stress $\boldsymbol{\sigma}$ and the thermodynamical force $\boldsymbol{A}_i$ associated to the internal variable $\boldsymbol{\alpha}_i$ are given by

$$\boldsymbol{\sigma} = \frac{\partial \psi}{\partial \boldsymbol{\varepsilon}}(\boldsymbol{\varepsilon}, \boldsymbol{\alpha}_1, \boldsymbol{\alpha}_2) \ , \boldsymbol{A}_i = -\frac{\partial \psi}{\partial \boldsymbol{\alpha}_i}(\boldsymbol{\varepsilon}, \boldsymbol{\alpha}_1, \boldsymbol{\alpha}_2). \tag{1}$$

The evolution law of internal variables $\boldsymbol{\alpha}_1$ and $\boldsymbol{\alpha}_2$ is given by the normality flow rule

$$(\dot{\boldsymbol{\alpha}}_1, \dot{\boldsymbol{\alpha}}_2) \in \partial\mathcal{C}(\boldsymbol{A}_1, \boldsymbol{A}_2) \tag{2}$$

where the superscript $\dot{}$ denotes the left-time derivative, e.g. $\dot{\boldsymbol{\alpha}}_1 = \lim_{\delta t \to 0^+}[\boldsymbol{\alpha}_1(t) - \boldsymbol{\alpha}_1(t-\delta t)]/\delta t$. In (2), $\partial\mathcal{C}$ denotes the normal cone defined by

$$\begin{aligned}\partial\mathcal{C}(\boldsymbol{A}_1, \boldsymbol{A}_2) = \quad \big\{(\boldsymbol{n}_1, \boldsymbol{n}_2) \in \mathrm{dev}(\mathbb{R}^{3\times3}_s)^2 | (\boldsymbol{A}_1 - \boldsymbol{A}'_1) : \boldsymbol{n}_1 + (\boldsymbol{A}_2 - \boldsymbol{A}'_2) : \boldsymbol{n}_2 \geq 0 \\ \forall (\boldsymbol{A}'_1, \boldsymbol{A}'_2) \in \mathcal{C}\big\}.\end{aligned} \tag{3}$$

In (3), the symbol : denotes the contraction with respect to the last two indices, e.g. $\boldsymbol{A} : \boldsymbol{A}' = \sum_{ij} A_{ij} A'_{ji}$. With a slight abuse of notations, we will use the same symbol : for tensors in the product space $\mathrm{dev}(\mathbb{R}^{3\times3}_s) \times \mathrm{dev}(\mathbb{R}^{3\times3}_s)$, e.g.

$$(\boldsymbol{A}_1, \boldsymbol{A}_2) : (\boldsymbol{A}'_1, \boldsymbol{A}'_2) = \boldsymbol{A}_1 : \boldsymbol{A}'_1 + \boldsymbol{A}_2 : \boldsymbol{A}'_2$$

with $\boldsymbol{A}_i$ and $\boldsymbol{A}'_i$ in $\mathrm{dev}(\mathbb{R}^{3\times3}_s)$. From (2) and (3) we have

$$(\dot{\boldsymbol{\alpha}}_1, \dot{\boldsymbol{\alpha}}_2) : (\boldsymbol{A}_1 - \boldsymbol{A}'_1, \boldsymbol{A}_2 - \boldsymbol{A}'_2) \geq 0 \ \forall (\boldsymbol{A}'_1, \boldsymbol{A}'_2) \in \mathcal{C}. \tag{4}$$

Eq. (4) corresponds to the principle of maximum dissipation. Following standard requirements, the origin is assumed to be in the interior of the elasticity domain $\mathcal{C}$, i.e. there exists $r > 0$ such that

$$\{\boldsymbol{A} \in \mathrm{dev}(\mathbb{R}^{3\times3}_s) | r \geq \|\boldsymbol{A}\|\} \subset \mathcal{C}. \tag{5}$$

The norm $\|\cdot\|$ in (5) is the Euclidean norm, e.g. $\|\boldsymbol{A}\| = \sqrt{\boldsymbol{A} : \boldsymbol{A}}$.

Extended versions of Eqs (1) and (2) are needed for our purpose. A distinctive feature of constitutive models involving phase transformation is indeed that the variable $\boldsymbol{\alpha}_1$ is constrained to take values in a given bounded set $\mathcal{T}_1$, i.e. we have a requirement of the form

$$\boldsymbol{\alpha}_1 \in \mathcal{T}_1 \tag{6}$$

where the set $\mathcal{T}_1 \subset \mathrm{dev}(\mathbb{R}^{3\times3}_s)$ is assumed to be closed and convex. Such a constraint follows from the mass conservation in the phase transformation process. The normality flow rule (2) needs to be amended in order to account for the constraint (6) on the internal variable $\boldsymbol{\alpha}_1$. In more detail, Eq. (2) needs to be replaced by

$$\begin{aligned}\boldsymbol{A}_1 &= \boldsymbol{A}_1^d + \boldsymbol{A}_1^r, \\ (\dot{\boldsymbol{\alpha}}_1, \dot{\boldsymbol{\alpha}}_2) &\in \partial\mathcal{C}(\boldsymbol{A}_1^d, \boldsymbol{A}_2), \\ \boldsymbol{A}_1^r &\in \partial\mathcal{T}_1(\boldsymbol{\alpha}_1),\end{aligned} \tag{7}$$

where $\partial\mathcal{T}_1$ is the normal cone to $\mathcal{T}_1$, defined in a way similar to (3). We refer e.g. to Frémond (2002) for a derivation of (7) from the principle of thermodynamics. The term $\boldsymbol{A}_1^r$ in (7) can be interpreted as a reaction force associated with the constraint (6). In particular, $\boldsymbol{A}_1^r$ vanishes if $\boldsymbol{\alpha}_1$ is in the interior of $\mathcal{T}_1$.

An extended form of Eq. (1) is also needed. In the definition of $\boldsymbol{A}_i$ in (1), it is indeed assumed implicitly that ψ is differentiable with respect to $\boldsymbol{\alpha}_i$. However, some models of phase transformation consider an energy function that is only *subdifferentiable* with respect to $\boldsymbol{\alpha}_i$ (some examples will be provided later on). In such case, the thermodynamical force $\boldsymbol{A}_i$ is given by

$$-(\boldsymbol{A}_1, \boldsymbol{A}_2) \in \partial_{\boldsymbol{\alpha}} \psi(\boldsymbol{\varepsilon}, \boldsymbol{\alpha}_1, \boldsymbol{\alpha}_2) \tag{8}$$

where $\partial_{\boldsymbol{\alpha}}\psi$ is the subdifferential of ψ with respect to $\boldsymbol{\alpha} = (\boldsymbol{\alpha}_1, \boldsymbol{\alpha}_2)$, i.e. $\partial_{\boldsymbol{\alpha}}\psi(\boldsymbol{\varepsilon}, \boldsymbol{\alpha}_1, \boldsymbol{\alpha}_2)$ is the set of values $(\boldsymbol{U}_1, \boldsymbol{U}_2) \in \mathrm{dev}(\mathbb{R}_s^{3\times 3})^2$ that verify

$$(\boldsymbol{\alpha}_1' - \boldsymbol{\alpha}_1, \boldsymbol{\alpha}_2' - \boldsymbol{\alpha}_2) : (\boldsymbol{U}_1, \boldsymbol{U}_2) \leq \psi(\boldsymbol{\varepsilon}, \boldsymbol{\alpha}_1', \boldsymbol{\alpha}_2') - \psi(\boldsymbol{\varepsilon}, \boldsymbol{\alpha}_1, \boldsymbol{\alpha}_2) \tag{9}$$

for all $(\boldsymbol{\alpha}_1', \boldsymbol{\alpha}_2')$.

In this paper, we consider free energy functions ψ of the form

$$\psi(\boldsymbol{\varepsilon}, \boldsymbol{\alpha}_1, \boldsymbol{\alpha}_2) = \frac{1}{2}(\boldsymbol{\varepsilon} - \mathbb{K}_1 : \boldsymbol{\alpha}_1 - \mathbb{K}_2 : \boldsymbol{\alpha}_2) : \mathbb{L} : (\boldsymbol{\varepsilon} - \mathbb{K}_1 : \boldsymbol{\alpha}_1 - \mathbb{K}_2 : \boldsymbol{\alpha}_2) + f(\boldsymbol{\alpha}_1, \boldsymbol{\alpha}_2) + h(\boldsymbol{\alpha}_1) \tag{10}$$

where

- $\mathbb{L}$ is a symmetric positive definite fourth-order tensor.
- $\mathbb{K}_1$ and $\mathbb{K}_2$ are fourth-order tensors (not necessarily symmetric nor positive).
- f is convex, positive and Hadamard directionally differentiable.
- h is differentiable and positive (but not necessarily convex).

Since f is convex, it is subdifferentiable and admits a directional derivative $f'(\boldsymbol{\alpha}; \boldsymbol{U})$ in any admissible direction $\boldsymbol{U}$, given by

$$f'(\boldsymbol{\alpha}; \boldsymbol{U}) = \lim_{t \longrightarrow 0^+} \frac{f(\boldsymbol{\alpha} + \delta t\, \boldsymbol{U}) - f(\boldsymbol{\alpha})}{\delta t}.$$

The requirement that f is Hadamard differentiable means that

$$f'(\boldsymbol{\alpha}; \boldsymbol{U}) = \lim_{n \to \infty} \frac{f(\boldsymbol{\alpha} + t_n \boldsymbol{U}_n) - f(\boldsymbol{\alpha})}{t_n} \tag{11}$$

for any sequence $\{t_n\}$ converging towards 0^+ and any sequence $\{\boldsymbol{U}_n\}$ such that $\boldsymbol{U}_n \to \boldsymbol{U}$ as $n \to \infty$ (Flett, 1980).

With the form (10) of the free energy, expression (1) of the stress becomes

$$\boldsymbol{\sigma} = \mathbb{L} : (\boldsymbol{\varepsilon} - \mathbb{K}_1 : \boldsymbol{\alpha}_1 - \mathbb{K}_2 : \boldsymbol{\alpha}_2). \tag{12}$$

The total strain $\boldsymbol{\varepsilon}$ thus decomposes as the sum of the elastic strain $\mathbb{L}^{-1} : \boldsymbol{\sigma}$ and inelastic strains $\mathbb{K}_i : \boldsymbol{\alpha}_i$ $(i = 1, 2)$. The constitutive relation (8) can be written as

$$(\boldsymbol{A}_1, \boldsymbol{A}_2) \in (\mathbb{K}_1^T : \boldsymbol{\sigma}, \mathbb{K}_2^T : \boldsymbol{\sigma}) - (h'(\boldsymbol{\alpha}_1), 0) - \partial f \tag{13}$$

where $\mathbb{K}_i^T$ is the transpose of $\mathbb{K}_i$ and ∂f is the subdifferential of f, defined in a way similar to (9).

As mentioned in the introduction, the class of constitutive models considered is motivated by existing models of phase transformation with permanent inelasticity. Some illustrative examples are presented next.

2.1. Model of Auricchio et al. (2007)

With the present set of notations, the set $\mathcal{T}_1$ corresponding to the model of Auricchio et al. (2007) is

$$\mathcal{T}_1 = \{\boldsymbol{\alpha}_1 \in \mathrm{dev}(\mathbb{R}^{3\times 3}_s) | \varepsilon_L \geq \|\boldsymbol{\alpha}_1\|\} \tag{14}$$

where ε_L is a material parameter. The free energy ψ considered by Auricchio et al. (2007) is

$$\psi = \frac{1}{2}K\theta^2 + G\|\boldsymbol{e} - \boldsymbol{\alpha}_1\|^2 + \tau_M\|\boldsymbol{\alpha}_1 - \boldsymbol{\alpha}_2\| + \frac{1}{2}H_1\|\boldsymbol{\alpha}_1\|^2 + \frac{1}{2}H_2\|\boldsymbol{\alpha}_2\|^2 - A\boldsymbol{\alpha}_1 : \boldsymbol{\alpha}_2 \tag{15}$$

where θ and $\boldsymbol{e}$ are the hydrostatic and the deviatoric part of the total strain $\boldsymbol{\varepsilon}$; τ_M is a positive material parameter depending on temperature; H_1, H_2 and A define respectively the hardening of phase transformation, the saturation of the permanent inelastic strain evolution, and model degradation (see Fig. 1). The internal variable $\boldsymbol{\alpha}_1$ is the transformation strain[1]and the variable $\boldsymbol{\alpha}_2$ is the permanent inelastic strain[2]. Let $\mathbb{I}$ be the fourth-order unit tensor and define

$$\mathbb{J} = (\mathbf{1} \otimes \mathbf{1})/3, \quad \mathbb{K} = \mathbb{I} - \mathbb{J} \tag{16}$$

[1]denoted by $\boldsymbol{\varepsilon}^{tr}$ in the paper by Auricchio et al. (2007)

[2]denoted by $\boldsymbol{q}$ in the paper by Auricchio et al. (2007)

where $\mathbf{1}$ is the second-order unit tensor The function (15) can be put in the form (10) by setting $\mathbb{L} = 3K\mathbb{J} + 2G\mathbb{K}$, $\mathbb{K}_1 = \mathbb{K}$, $\mathbb{K}_2 = 0$, $h = 0$. The corresponding function f is

$$f(\boldsymbol{\alpha}_1, \boldsymbol{\alpha}_2) = \tau_M \|\boldsymbol{\alpha}_1 - \boldsymbol{\alpha}_2\| + \frac{1}{2} H_1 \|\boldsymbol{\alpha}_1\|^2 + \frac{1}{2} H_2 \|\boldsymbol{\alpha}_2\|^2 - A\boldsymbol{\alpha}_1 : \boldsymbol{\alpha}_2. \tag{17}$$

It can be verified that the function f in (17) is positive and convex if

$$H_1 \geq 0 \;\; H_2 \geq 0 \;, \;\; H_1 H_2 - A^2 \geq 0. \tag{18}$$

Typical values used in Auricchio et al. (2007) are $H_1 = 1000$ MPa, $H_2 = 15000$ MPa, $A = 2000$ MPa, which satisfy (18).

Observe that the function f in (17) is not differentiable because of the term $\|\boldsymbol{\alpha}_1 - \boldsymbol{\alpha}_2\|$. It can be verified, however, that the function f in (17) is Hadamard directionally differentiable. The subdifferential $\partial f(\boldsymbol{\alpha}_1, \boldsymbol{\alpha}_2)$ is given by

$$\partial f(\boldsymbol{\alpha}_1, \boldsymbol{\alpha}_2) = \begin{cases} \tau_M \dfrac{(\boldsymbol{\alpha}_1 - \boldsymbol{\alpha}_2, \boldsymbol{\alpha}_2 - \boldsymbol{\alpha}_1)}{\|\boldsymbol{\alpha}_1 - \boldsymbol{\alpha}_2\|} + (H_1\boldsymbol{\alpha}_1 - A\boldsymbol{\alpha}_2, H_2\boldsymbol{\alpha}_2 - A\boldsymbol{\alpha}_1) \\ \qquad\qquad\qquad\qquad\qquad\qquad\qquad\qquad\qquad\qquad \text{if } \boldsymbol{\alpha}_1 \neq \boldsymbol{\alpha}_2, \\ \{\tau_M(\boldsymbol{\tau}, -\boldsymbol{\tau}) | \operatorname{tr} \boldsymbol{\tau} = 0, \|\boldsymbol{\tau}\| \leq 1\} + (H_1\boldsymbol{\alpha}_1 - A\boldsymbol{\alpha}_2, H_2\boldsymbol{\alpha}_2 - A\boldsymbol{\alpha}_1) \\ \qquad\qquad\qquad\qquad\qquad\qquad\qquad\qquad\qquad\qquad \text{if } \boldsymbol{\alpha}_1 = \boldsymbol{\alpha}_2. \end{cases} \tag{19}$$

The elasticity domain $\mathcal{C}$ originally considered by Auricchio et al. (2007) is defined by the equation

$$\|\boldsymbol{A}_1\| + \kappa \|\boldsymbol{A}_2\| \leq R \tag{20}$$

where κ and R are non-negative material parameters. The term $\|\boldsymbol{A}_1\| + \kappa\|\boldsymbol{A}_2\|$ in (20) is a weighted taxicab norm of $(\boldsymbol{A}_1, \boldsymbol{A}_2)$. As pointed out by Barrera et al. (2014), other norms can be chosen for defining the elasticity domain. In particular, replacing the weighted taxicab norm in (20) with a weighted Euclidean norm leads to results that are more consistent with experiments. In that case the elasticity domain is defined by

$$\|\boldsymbol{A}_1\|^2 + \kappa^2 \|\boldsymbol{A}_2\|^2 \leq R^2. \tag{21}$$

In Fig. 1 are plotted some stress-strain curves illustrating the role of the main material parameters on functional fatigue. Fig. 1(a) corresponds to the original Souza-Auricchio model (Souza et al., 1998; Auricchio and Petrini, 2004a) which is recovered from (15) by removing the variable $\boldsymbol{\alpha}_2$. Fig. 1(a) shows the stress-strain curve for a stress-driven uniaxial loading cycle with a maximum applied stress of 400 MPa. Values of the material parameters are $E = 50000$ MPa, $\nu = 0.28$, $\tau_M = 150$

MPa, $H_1 = 1000$ MPa, $R = 50$ MPa, $\epsilon_L = 0.04$ (we keep the same values for all the curves in Fig. 1). The curve in Fig. 1(a) corresponds to the superelastic regime of the material. At the end of the loading cycle, the internal variable $\boldsymbol{\alpha}_1$ restores to its initial value $\boldsymbol{\alpha}_1 = 0$, so that there is no degradation effects over subsequent cycles: the stress-strain curve remains identical to that shown in Fig. 1(a). To illustrate the role played by the internal variable $\boldsymbol{\alpha}_2$ in the model of Auricchio et al. (2007), 50 stress-driven loading cycles with a maximum applied of stress of 400 MPa have been simulated numerically. The expression (21) of the elasticity domain was adopted and the algorithm of Peigney et al. (2018) was used for solving the incremental problem at each time step. In Fig. 1(b) is shown the stress-strain response obtained for $\kappa = 10$ and $H_2 = A = 0$ (the stress-strain curve corresponding to the last loading cycle is shown in red). We can observe the build-up of a permanent inelastic strain over the consecutive loading cycles. The material parameter H_2 in (15) controls the saturation of the permanent inelastic strain as illustrated in Fig. 1(c) showing the stress-strain response for $H_2 = 15000$ MPa and $A = 0$. The material parameter A in (15) controls the decrease of the stress plateaux as illustrated in Fig 1(d) showing the results for $H_2 = 15000$ MPa and $A = 2000$ MPa. In Figs. 1(c) and (d), the convergence of the stress-strain curve towards a steady-state cycle can be observed.

2.2. Model of Barrera et al. (2014)

Barrera et al. (2014) considered an energy function ψ of the form

$$\psi = \frac{1}{2}K\theta^2 + G\|\boldsymbol{e} - \boldsymbol{e}^{tr} - a\boldsymbol{q}\|^2 + \tau_M\|\boldsymbol{e}^{tr} - \boldsymbol{q}\| + \frac{1}{2}H\|\boldsymbol{q}\|^2 + \frac{1}{2}H'\|\boldsymbol{e}^{tr} - \boldsymbol{q}\|^2 \quad (22)$$

where $\boldsymbol{e}^{tr}$ and $\boldsymbol{q}$ are internal variables constrained to live in the set

$$\{(\boldsymbol{e}^{tr}, \boldsymbol{q}) \in \mathrm{dev}(\mathbb{R}^{3\times3}_s)^2 | \epsilon_L \geq \|\boldsymbol{e}^{tr} - \boldsymbol{q}\|\}. \quad (23)$$

In the original work by Barrera et al. (2014), the parameter ϵ_L in (23) evolves with $\boldsymbol{e}^{tr}$ and $\boldsymbol{q}$. Here we consider a simplified version of the model in which ϵ_L is a fixed material parameter. Let$(\boldsymbol{X}, \boldsymbol{Q})$ be the thermodynamical forces associated to $(\boldsymbol{e}^{tr}, \boldsymbol{q})$, i.e.

$$-(\boldsymbol{X}, \boldsymbol{Q}) \in \partial_{(\boldsymbol{e}^{tr}, \boldsymbol{q})}\psi.$$

Barrera et al. (2014) considered an elasticity domain of the form

$$\max(\|\boldsymbol{X}\|, \kappa\|\boldsymbol{Q}\|) \leq R. \quad (24)$$

In the case where $(\boldsymbol{e}^{tr}, \boldsymbol{q})$ is in the interior of the domain defined by (23), we recall that the flow rule is prescribed by the maximum dissipation principle

$$0 \leq (\dot{\boldsymbol{e}}^{tr}, \dot{\boldsymbol{q}}) : (\boldsymbol{X} - \boldsymbol{X}', \boldsymbol{Q} - \boldsymbol{Q}') \quad (25)$$

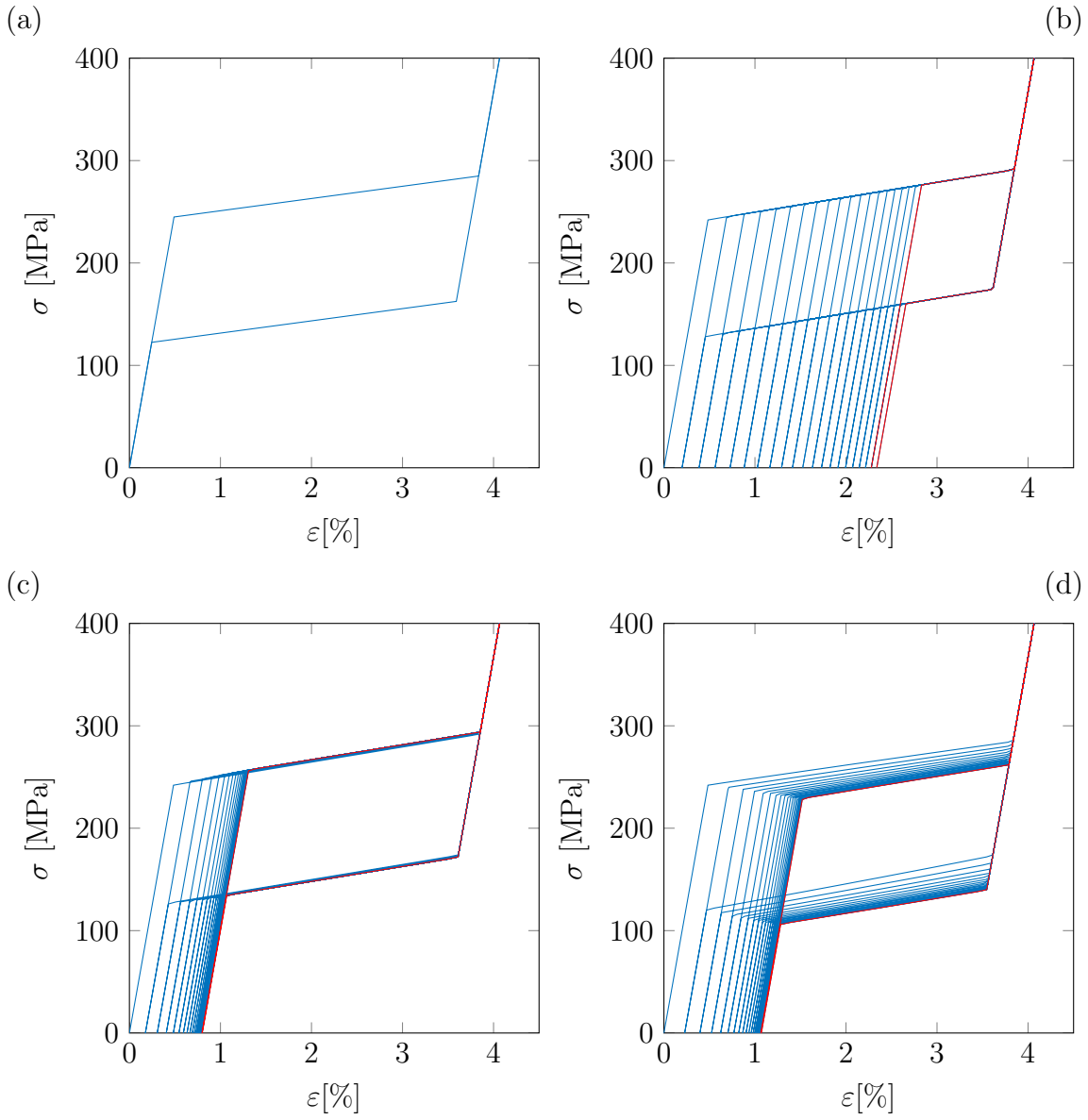

Figure 1: Stress-strain curves for a cyclic stress-driven uniaxial loading. Souza-Auricchio model (a). Model of Auricchio et al. (2007) with $H_2 = A = 0$ (b), H_2=15000 MPa, $A = 0$ (c), $H_2 = 15000$ MPa, $A = 2000$ MPa (d).

for any $(\boldsymbol{X}', \boldsymbol{Q}')$ in the elasticity domain defined by (24). In contrast with the model of Auricchio et al. (2007), the model of Barrera et al. (2014) cannot be put in the format (6)-(7)-(8)-(10) by simply identifying $(\boldsymbol{\alpha}_1, \boldsymbol{\alpha}_2)$ with $(\boldsymbol{e}^{tr}, \boldsymbol{q})$. A less direct

change of variables is needed, as is now described . Define $(\boldsymbol{\alpha}_1, \boldsymbol{\alpha}_2)$ as

$$\boldsymbol{\alpha}_1 = \boldsymbol{e}^{tr} - \boldsymbol{q},\ \boldsymbol{\alpha}_2 = -\boldsymbol{e}^{tr}. \tag{26}$$

The relation (26) can be inverted as

$$\boldsymbol{e}^{tr} = -\boldsymbol{\alpha}_2,\ \boldsymbol{q} = -\boldsymbol{\alpha}_1 - \boldsymbol{\alpha}_2. \tag{27}$$

That change of variables allows constraint (23) to be rewritten as $\boldsymbol{\alpha}_1 \in \mathcal{T}_1$ where $\mathcal{T}_1$ is the bounded set defined as in (14). The energy function (22) can be rewritten in terms of $(\boldsymbol{\alpha}_1, \boldsymbol{\alpha}_2)$ as

$$\psi = \frac{1}{2}K\theta^2 + G\|\boldsymbol{e} + a\boldsymbol{\alpha}_1 + (1+a)\boldsymbol{\alpha}_2\|^2 + \tau_M\|\boldsymbol{\alpha}_1\| + \frac{1}{2}H\|\boldsymbol{\alpha}_1 + \boldsymbol{\alpha}_2\|^2 + \frac{1}{2}H'\|\boldsymbol{\alpha}_1\|^2. \tag{28}$$

Expression (28) can be put in the form (10) by setting $\mathbb{L} = 3K\mathbb{J} + 2G\mathbb{K}$, $\mathbb{K}_1 = -a\mathbb{K}$, $\mathbb{K}_2 = -(1+a)\mathbb{K}$, $h(\boldsymbol{\alpha}_1) = \tau_M\|\boldsymbol{\alpha}_1\| + \frac{1}{2}H'\|\boldsymbol{\alpha}_1\|^2$ and

$$f(\boldsymbol{\alpha}_1, \boldsymbol{\alpha}_2) = \frac{1}{2}H\|\boldsymbol{\alpha}_1 + \boldsymbol{\alpha}_2\|^2. \tag{29}$$

The function f in (29) is convex, positive and can easily be verified to be Hadamard directionally differentiable. A direct calculation shows that the thermodynamical forces $(\boldsymbol{A}_1, \boldsymbol{A}_2)$ associated to $(\boldsymbol{\alpha}_1, \boldsymbol{\alpha}_2)$ are related to the thermodynamical forces $(\boldsymbol{X}, \boldsymbol{Q})$ associated to $(\boldsymbol{e}^{tr}, \boldsymbol{q})$ by

$$\boldsymbol{A}_1 = -\boldsymbol{Q}, \boldsymbol{A}_2 = -\boldsymbol{X} - \boldsymbol{Q} \tag{30}$$

or, equivalently,

$$\boldsymbol{X} = \boldsymbol{A}_1 - \boldsymbol{A}_2, \boldsymbol{Q} = -\boldsymbol{A}_1. \tag{31}$$

As a consequence of (24) and (30), $(\boldsymbol{A}_1, \boldsymbol{A}_2)$ needs to live in the elasticity domain $\mathcal{C}$ defined by

$$\max(\|\boldsymbol{A}_1 - \boldsymbol{A}_2\|, \kappa\|\boldsymbol{A}_1\|) \leq R. \tag{32}$$

Using (27) and (31), the flow rule (25) can be rewritten as

$$0 \leq (-\dot{\boldsymbol{\alpha}}_2, -\dot{\boldsymbol{\alpha}}_1 - \dot{\boldsymbol{\alpha}}_2) : (\boldsymbol{A}_1 - \boldsymbol{A}_1' - \boldsymbol{A}_2 + \boldsymbol{A}_2', -\boldsymbol{A}_1 + \boldsymbol{A}_1') \tag{33}$$

for any $(\boldsymbol{A}_1', \boldsymbol{A}_2')$ in $\mathcal{C}$. Expanding the right-hand side of (33) gives

$$0 \leq (\dot{\boldsymbol{\alpha}}_1, \dot{\boldsymbol{\alpha}}_2) : (\boldsymbol{A}_1 - \boldsymbol{A}_1', \boldsymbol{A}_2 - \boldsymbol{A}_2') \tag{34}$$

for any $(\boldsymbol{A}_1', \boldsymbol{A}_2') \in \mathcal{C}$. Eq. (34) corresponds to the normality flow rule for the variable $(\boldsymbol{\alpha}_1, \boldsymbol{\alpha}_2)$ with an elasticity domain defined by (32). In summary, defining $(\boldsymbol{\alpha}_1, \boldsymbol{\alpha}_2)$ as (26) allows the model of Barrera et al. (2014) to be cast in the format defined by Eqs (6)-(7)-(8)-(10). The corresponding expression of $\mathcal{T}_1$, ψ and $\mathcal{C}$ are given by (14), (28) and (32) respectively.

3. Quasi-static evolution of a continuum

Consider a continuum occupying a domain Ω and submitted to a loading history represented by body forces $\boldsymbol{f}^d$, displacements $\boldsymbol{u}^d$ imposed on a part Γ_u of the boundary Γ and tractions $\boldsymbol{T}^d$ prescribed on $\Gamma_T = \Gamma - \Gamma_u$. The given functions $\boldsymbol{f}^d$, $\boldsymbol{u}^d$, $\boldsymbol{T}^d$ depend on position $\boldsymbol{x}$ and time t. In order to alleviate the expressions, this dependence will be omitted in the notations unless in the case of possible ambiguities. Assuming quasi-static evolutions, the stress field $\boldsymbol{\sigma}(t)$ and the strain field $\boldsymbol{\varepsilon}(t)$ at time t need to be respectively in the sets

$$\mathcal{K}_\sigma(t) = \{\boldsymbol{\sigma} | \operatorname{div} \boldsymbol{\sigma} + \boldsymbol{f}^d(t) = 0 \text{ in } \Omega; \boldsymbol{\sigma} \cdot \boldsymbol{n} = \boldsymbol{T}^d(t) \text{ on } \Gamma_T\}$$

and

$$\mathcal{K}_\epsilon(t) = \{\boldsymbol{\varepsilon} | \boldsymbol{\varepsilon} = (\nabla \boldsymbol{u} + \nabla^T \boldsymbol{u})/2 \text{ in } \Omega;\ \boldsymbol{u} = \boldsymbol{u}^d(t) \text{ on } \Gamma_u\}.$$

The local constitutive equations presented in Sect. 2 need to be satisfied at each point. It is convenient to use the compact notations $\boldsymbol{\alpha} = (\boldsymbol{\alpha}_1, \boldsymbol{\alpha}_2)$, $\boldsymbol{A} = (\boldsymbol{A}_1, \boldsymbol{A}_2)$, $\boldsymbol{A}^d = (\boldsymbol{A}_1^d, \boldsymbol{A}_2)$, $\boldsymbol{A}^r = (\boldsymbol{A}_1^r, 0)$. The gradient of the function h with respect to $\boldsymbol{\alpha}$ is denoted by ∇h, i.e $\nabla h = (h'(\boldsymbol{\alpha}_1), 0)$. We also introduce the linear operator $\mathbb{K}$ defined on $\operatorname{dev}(\mathbb{R}^{3\times3}_s)^2$ by the relation $\mathbb{K} : \boldsymbol{\alpha} = \mathbb{K}_1 : \boldsymbol{\alpha}_1 + \mathbb{K}_2 : \boldsymbol{\alpha}_2$. Eqs. (12) and (13) can be rewritten in the compact form

$$\begin{array}{c} \boldsymbol{\sigma} = \mathbb{L} : (\boldsymbol{\varepsilon} - \mathbb{K} : \boldsymbol{\alpha}) \ , \\ \mathbb{K}^T : \boldsymbol{\sigma} - \nabla h(\boldsymbol{\alpha}) \in \boldsymbol{A} + \partial f(\boldsymbol{\alpha}) \end{array} \tag{35}$$

where $\mathbb{K}^T$ is the transpose of $\mathbb{K}$ (so that $\boldsymbol{\sigma} : \mathbb{K} : \boldsymbol{A} = \boldsymbol{A} : \mathbb{K}^T : \boldsymbol{\sigma}$ for any $\boldsymbol{\sigma} \in \mathbb{R}^{3\times3}_s$ and $\boldsymbol{A} \in (\operatorname{dev}(\mathbb{R}^{3\times3}_s))^2$).

Quasi-static evolutions of the continuum are governed by the following system:

$$\begin{array}{c} \boldsymbol{\sigma} \in \mathcal{K}_\sigma \ , \ \boldsymbol{\varepsilon} \in \mathcal{K}_\epsilon \ , \ \boldsymbol{\alpha} \in \mathcal{T}, \\ \dot{\boldsymbol{\alpha}} \in \partial \mathcal{C}(\boldsymbol{A}^d) \ , \ \boldsymbol{A}^r \in \partial \mathcal{T}(\boldsymbol{\alpha}), \ \boldsymbol{B} \in \partial f(\boldsymbol{\alpha}) \\ \boldsymbol{\sigma} = \mathbb{L} : (\boldsymbol{\varepsilon} - \mathbb{K} : \boldsymbol{\alpha}), \\ \mathbb{K}^T : \boldsymbol{\sigma} - \nabla h(\boldsymbol{\alpha}) = \boldsymbol{A}^d + \boldsymbol{A}^r + \boldsymbol{B}, \end{array} \tag{36}$$

where $\mathcal{T}$ is the subset of $(\operatorname{dev}(\mathbb{R}^{3\times3}_s))^2$ defined by $\mathcal{T} = \mathcal{T}_1 \times \operatorname{dev}(\mathbb{R}^{3\times3}_s)$. For later reference, note that any $\boldsymbol{A}^r \in \partial \mathcal{T}(\boldsymbol{\alpha})$ is of the form $\boldsymbol{A}^r = (\boldsymbol{A}_1^r, 0)$ with $\boldsymbol{A}_1^r \in \partial I_{\mathcal{T}_1}(\boldsymbol{\alpha}_1)$.

We introduce the so-called *fictitious elastic response* $(\boldsymbol{\sigma}^E, \boldsymbol{\varepsilon}^E)$ of the continuum, defined as the solution to the linear elasticity problem

$$\boldsymbol{\sigma}^E \in \mathcal{K}_\sigma \ , \boldsymbol{\varepsilon}^E \in \mathcal{K}_\epsilon \ , \boldsymbol{\sigma}^E = \mathbb{L} : \boldsymbol{\varepsilon}^E. \tag{37}$$

Setting $\boldsymbol{\rho} = \boldsymbol{\sigma} - \boldsymbol{\sigma}^E$ and noting that $\boldsymbol{\varepsilon} = \boldsymbol{\varepsilon}^E + \mathbb{L}^{-1} : \boldsymbol{\rho} + \mathbb{K} : \boldsymbol{\alpha}$, system (36) can be recast as

$$\begin{gathered} \boldsymbol{\rho} \in \mathcal{K}_\sigma^0 \ , \ \boldsymbol{\alpha} \in \mathcal{T}, \\ \dot{\boldsymbol{\alpha}} \in \partial \mathcal{C}(\boldsymbol{A}^d) \ , \ \boldsymbol{A}^r \in \partial \mathcal{T}(\boldsymbol{\alpha}), \ \boldsymbol{B} \in \partial f(\boldsymbol{\alpha}), \\ \mathbb{L}^{-1} : \boldsymbol{\rho} + \mathbb{K} : \boldsymbol{\alpha} \in \mathcal{K}_\epsilon^0, \\ \mathbb{K}^T : (\boldsymbol{\sigma}^E + \boldsymbol{\rho}) - \nabla h(\boldsymbol{\alpha}) = \boldsymbol{A}^d + \boldsymbol{A}^r + \boldsymbol{B}, \end{gathered} \tag{38}$$

where the sets $\mathcal{K}_\sigma^0$ and $\mathcal{K}_\epsilon^0$ are defined by

$$\begin{aligned} \mathcal{K}_\sigma^0 &= \{\boldsymbol{\sigma} | \operatorname{div} \boldsymbol{\sigma} = 0 \text{ in } \Omega; \boldsymbol{\sigma} \cdot \boldsymbol{n} = 0 \text{ on } \Gamma_T\}, \\ \mathcal{K}_\epsilon^0 &= \{\boldsymbol{\varepsilon} | \boldsymbol{\varepsilon} = (\nabla \boldsymbol{u} + \nabla^T \boldsymbol{u})/2 \text{ in } \Omega; \ \boldsymbol{u} = 0 \text{ on } \Gamma_u\}. \end{aligned} \tag{39}$$

For later reference, note that

$$\int_\Omega \boldsymbol{\sigma} : \boldsymbol{\varepsilon} dv = 0 \text{ for any } \boldsymbol{\sigma} \in \mathcal{K}_\sigma^0 \text{ and } \boldsymbol{\varepsilon} \in \mathcal{K}_\epsilon^0. \tag{40}$$

Eq. (38) prescribes the evolution of the system starting from a given initial state. Elastic solutions to (38) are characterized by the fact that $\dot{\boldsymbol{\alpha}} = 0$ and therefore satisfy

$$\mathbb{K}^T : (\boldsymbol{\sigma}^E(\boldsymbol{x}, t) + \boldsymbol{\rho}(x)) - \nabla h(\boldsymbol{\alpha}) - \boldsymbol{B} - \boldsymbol{A}^r \in \mathcal{C} \tag{41}$$

where $\boldsymbol{\rho} \in \mathcal{K}_\sigma^0$ is time-independent, $\boldsymbol{A}^r \in \partial \mathcal{T}(\boldsymbol{\alpha})$, $\boldsymbol{B} \in \partial f(\boldsymbol{\alpha})$. Since $\partial f(\boldsymbol{\alpha})$ and $\partial \mathcal{T}(\boldsymbol{\alpha})$ are multi-valued, $\boldsymbol{A}^r$ and $\boldsymbol{B}$ in (41) may depend on time even though $\boldsymbol{\alpha}$ is time-independent. In the following we are interested in situations where shakedown occurs. The most intuitive definition of shakedown is that the evolution given by (38) becomes elastic in the large time limit, i.e. that the internal variable $\boldsymbol{\alpha}(\boldsymbol{x}, t)$ solving (38) converges towards a time-independent limit $\boldsymbol{\alpha}_\infty(\boldsymbol{x})$ as $t \to \infty$. For proving shakedown theorems, it is more convenient to use the energy-related definition that the dissipated energy $\int_0^T \int_\Omega \boldsymbol{A}^d : \dot{\boldsymbol{\alpha}} dt dv$ remains bounded with T. There is an intimate connection between those two definitions. In particular, the fact that the dissipated energy is bounded implies that $\boldsymbol{\alpha}(t)$ converges towards a time-independent limit. Let us briefly justify that statement: By (5) we have $r\boldsymbol{\alpha}(\dot{\boldsymbol{x}}, t)/\|\boldsymbol{\alpha}(\dot{\boldsymbol{x}}, t)\| \in \mathcal{C}$ for any $(\boldsymbol{x}, t)$. Using the principle of maximum dissipation (4) with $(\boldsymbol{A}_1^d, \boldsymbol{A}_2^d)$ and $(\boldsymbol{A}_1', \boldsymbol{A}_2') = r(\dot{\boldsymbol{\alpha}}_1, \dot{\boldsymbol{\alpha}}_2)/\|\dot{\boldsymbol{\alpha}}\|$, the inequality $r\|\dot{\boldsymbol{\alpha}}\| \leq \boldsymbol{A}^d : \dot{\boldsymbol{\alpha}}$ is obtained. It follows by integration that $\int_0^T \int_\Omega r\|\dot{\boldsymbol{\alpha}}\| dt dv \leq \int_0^T \int_\Omega \boldsymbol{A}^d : \dot{\boldsymbol{\alpha}} dt dv$. Consequently, if the dissipated energy remains bounded, then so is the norm $\int_0^T \int_\Omega \|\dot{\boldsymbol{\alpha}}\| dt dv$. Since the functional space $L_1(\Omega, \operatorname{dev}(\mathbb{R}_s^{3\times 3}))$ is a Banach space, the fact that $\int_0^T \int_\Omega \|\dot{\boldsymbol{\alpha}}\| dt dv$ remains bounded implies that $\boldsymbol{\alpha}(t)$ tends to a limit $\boldsymbol{\alpha}_\infty$ as $t \to \infty$.

4. Static approach

In standard plasticity, the well-known Melan's theorem gives a sufficient condition for shakedown (Melan, 1936; Koiter, 1960). With the notations adopted in this paper, standard plasticity corresponds to the special case $\mathcal{T}_1 = \mathrm{dev}(\mathbb{R}^{3\times3}_s)$, $\mathbb{K}_1 = \mathbb{K}$, $\mathbb{K}_2 = 0$, $f = h = 0$. The sufficient condition provided by Melan's theorem is

Condition 1. *There exists $m > 1$, $T > 0$ and a time-independent field $\boldsymbol{\rho}_* \in \mathcal{K}^0_\sigma$ such that $\mathbb{K}^T : (m\boldsymbol{\sigma}^E(\boldsymbol{x},t) + \boldsymbol{\rho}_*(x)) \in \mathcal{C}$ for all $\boldsymbol{x}$ in Ω and $t \geq T$.*

If Condition 1 is satisfied then Melan's theorem states that shakedown occurs for all initial states. In standard plasticity, fulfillment of Condition 1 amounts to assume that there exists an elastic solution (on the time interval $[T, +\infty)$) for the loading history $m\boldsymbol{f}^d$, $m\boldsymbol{u}^d$, $m\boldsymbol{T}^d$. From that interpretation and the characterization (41) of elastic solutions, it is tempting to conjecture that a sufficient shakedown condition for SMA models accounting for functional fatigue is the following

Condition 2. *There exists $m > 1$, $T > 0$, time-independent fields $(\boldsymbol{\rho}_*, \boldsymbol{\alpha}_*) \in \mathcal{K}^0_\sigma \times \mathcal{T}$ and some $\boldsymbol{A}^r_{1,*}(\boldsymbol{x},t) \in \mathrm{dev}(\mathbb{R}^{3\times3}_s)$, $\boldsymbol{B}_*(\boldsymbol{x},t) \in \partial f(\boldsymbol{\alpha}_*)$ such that*

$$\mathbb{K}^T : (m\boldsymbol{\sigma}^E(\boldsymbol{x},t) + \boldsymbol{\rho}_*(x)) - \nabla h(\boldsymbol{\alpha}_*) - \boldsymbol{B}_* - (\boldsymbol{A}^r_{1,*}, 0) \in \mathcal{C}$$

for all $\boldsymbol{x}$ in Ω and $t \geq T$.

That conjecture, however, turns out to be false in the general case. It is indeed possible to exhibit simple examples for which Condition 2 is satisfied but shakedown does not occur for all initial states (Peigney, 2010). In the case of pure phase-transformation (i.e. $\boldsymbol{\alpha}_1$ is the only internal variable), it has been proved that shakedown occurs for all initial states if Condition 2 is satisfied for some *time-independent* $\boldsymbol{A}^r_{1,*}$ (Peigney, 2010, 2014a). This motivates the introduction of the following condition as a candidate sufficient shakedown condition for SMA models accounting for functional fatigue:

Condition 3. *There exists $m > 1$, $T > 0$ and time-independent fields $(\boldsymbol{\rho}_*, \boldsymbol{\alpha}_*, \boldsymbol{A}^r_{1,*}, \boldsymbol{B}_*) \in \mathcal{K}^0_\sigma \times \mathcal{T} \times \mathrm{dev}(\mathbb{R}^{3\times3}_s) \times \partial f(\boldsymbol{\alpha}_*)$ such that*

$$\mathbb{K}^T : (m\boldsymbol{\sigma}^E(t) + \boldsymbol{\rho}_*) - \nabla h(\boldsymbol{\alpha}_*) - \boldsymbol{B}_* - (\boldsymbol{A}^r_{1,*}, 0) \in \mathcal{C} \tag{42}$$

for all $\boldsymbol{x}$ in Ω and $t \geq T$.

Condition 3 differs from Condition 2 by the fact that both $\boldsymbol{A}^r_{1,*}$ and $\boldsymbol{B}_*$ are required to be *time-independent*. In the following we prove that Condition 3 is indeed a sufficient condition for shakedown in the general case.

4.1. A sufficient condition for shakedown

Assume that Condition 3 is satisfied and let $(\boldsymbol{\rho}(\boldsymbol{x},t), \boldsymbol{\alpha}(\boldsymbol{x},t), \boldsymbol{A}^d(\boldsymbol{x},t), \boldsymbol{A}^r(\boldsymbol{x},t), \boldsymbol{B}(\boldsymbol{x},t))$ be a solution to the evolution problem (38) for some unspecified initial state $\boldsymbol{\alpha}(\boldsymbol{x},0)$. We define the dissipation $D(t)$ by

$$D(t) = \int_\Omega \boldsymbol{A}^d : \dot{\boldsymbol{\alpha}} dv \tag{43}$$

and we set

$$W(t) = \int_\Omega \frac{1}{2}\left[(\boldsymbol{\rho} - \frac{\boldsymbol{\rho}_*}{m}) : \mathbb{L}^{-1} : (\boldsymbol{\rho} - \frac{\boldsymbol{\rho}_*}{m}) + f(\boldsymbol{\alpha}) + h(\boldsymbol{\alpha})\right] dv. \tag{44}$$

The objective is to prove that shakedown occurs in the sense that the total dissipated energy $\int_0^T D(t)dt$ remains bounded in time T. For better clarity, the proof is broken down in 3 steps. The first step (Section 4.1.1) consists in relating the left-time derivative $\dot{W}(t)$ to the dissipation $D(t)$. The second step (Section 4.1.2) consists in deriving an upper bound on $\dot{W}(t)$. From there, time integration allows one to show that the dissipated energy $\int_0^T D(t)dt$ is bounded independently of T (Section 4.1.3).

4.1.1. Relation between $\dot{W}(t)$ and $D(t)$

Using the distinctive property $\dot{\boldsymbol{\rho}}_* = 0$ of Condition 3, a direct calculation yields

$$\dot{W}(t) = \int_\Omega \left[(\boldsymbol{\rho} - \frac{\boldsymbol{\rho}_*}{m}) : \mathbb{L}^{-1} : \dot{\boldsymbol{\rho}} + \dot{f} + \nabla h(\boldsymbol{\alpha}) : \dot{\boldsymbol{\alpha}}\right] dv$$

where $\dot{f}$ is the left-time derivative of $t \mapsto f(\boldsymbol{\alpha}(t))$, i.e.

$$\dot{f} = \lim_{t \longrightarrow 0^+} \frac{f(\boldsymbol{\alpha}(t)) - f(\boldsymbol{\alpha}(t-\delta t))}{\delta t}.$$

Note that

$$\dot{f} = -\lim_{t \longrightarrow 0^+} \frac{f(\boldsymbol{\alpha}(t) + \delta t\, \boldsymbol{U}(t)) - f(\boldsymbol{\alpha}(t))}{\delta t}$$

where $\boldsymbol{U}(t) = (\boldsymbol{\alpha}(t-\delta t) - \boldsymbol{\alpha}(t))/\delta t$. Since $\boldsymbol{U}(t) \longrightarrow -\dot{\boldsymbol{\alpha}}$ as $\delta t \longrightarrow 0^+$, property (11) yields

$$\dot{f} = -f'(\boldsymbol{\alpha}; -\dot{\boldsymbol{\alpha}}) \tag{45}$$

where $f'(\boldsymbol{\alpha}; -\dot{\boldsymbol{\alpha}})$ is the directional derivative in the direction $-\dot{\boldsymbol{\alpha}}$, evaluated at $\boldsymbol{\alpha}$. Eq. (38) shows that $\boldsymbol{\rho} - \boldsymbol{\rho}_*/m \in \mathcal{K}_\sigma^0$ and $\mathbb{L}^{-1} : \dot{\boldsymbol{\rho}} + \mathbb{K} : \dot{\boldsymbol{\alpha}} \in \mathcal{K}_\epsilon^0$. Property (40) then implies that

$$\int_\Omega (\boldsymbol{\rho} - \frac{\boldsymbol{\rho}_*}{m}) : (\mathbb{L}^{-1} : \dot{\boldsymbol{\rho}} + \mathbb{K} : \dot{\boldsymbol{\alpha}}) dv = 0. \tag{46}$$

Using (45) and (46), $\dot{W}(t)$ can be rewritten as

$$\dot{W}(t) = \int_\Omega \Big[-(\boldsymbol{\rho} - \frac{\boldsymbol{\rho}_*}{m}) : \mathbb{K} : \dot{\boldsymbol{\alpha}} - f'(\boldsymbol{\alpha}; -\dot{\boldsymbol{\alpha}}) + \nabla h(\boldsymbol{\alpha}) : \dot{\boldsymbol{\alpha}} \Big] \, dv$$

i.e.

$$\dot{W}(t) = \int_\Omega \Big[\Big(-\mathbb{K}^T : (\boldsymbol{\rho} - \frac{\boldsymbol{\rho}_*}{m}) + \nabla h(\boldsymbol{\alpha}) \Big) : \dot{\boldsymbol{\alpha}} - f'(\boldsymbol{\alpha}; -\dot{\boldsymbol{\alpha}}) \Big] \, dv.$$

Using the last equation in system (38), we obtain

$$\dot{W}(t) = -D(t) + \int_\Omega \Big[\Big(-\boldsymbol{A}^r - \boldsymbol{B} + \mathbb{K}^T : (\boldsymbol{\sigma}^E + \frac{\boldsymbol{\rho}_*}{m}) \Big) : \dot{\boldsymbol{\alpha}} - f'(\boldsymbol{\alpha}; -\dot{\boldsymbol{\alpha}}) \Big] \, dv \tag{47}$$

where $D(t)$ is the dissipation introduced in Eq. (43).

4.1.2. Bound on $\dot{W}(t)$

For a convex function $f(\boldsymbol{\alpha})$, we recall that the directional derivative $f'(\boldsymbol{\alpha}; \boldsymbol{U})$ satisfies (Hiriart-Urruty and Lemaréchal, 2001)

$$f'(\boldsymbol{\alpha}; \boldsymbol{U}) \geq \boldsymbol{U} : \boldsymbol{B}' \quad \forall \boldsymbol{B}' \in \partial f(\boldsymbol{\alpha}). \tag{48}$$

Using (48) with $\boldsymbol{U} = -\dot{\boldsymbol{\alpha}}$, we obtain

$$f'(\boldsymbol{\alpha}; -\dot{\boldsymbol{\alpha}}) + \boldsymbol{B} : \dot{\boldsymbol{\alpha}} \geq 0$$

where the property $\boldsymbol{B} \in \partial f(\boldsymbol{\alpha})$ has been used. It follows from (47) that

$$\dot{W}(t) \leq -D(t) + \int_\Omega \Big[-\boldsymbol{A}^r + \mathbb{K}^T : (\boldsymbol{\sigma}^E + \frac{\boldsymbol{\rho}_*}{m}) \Big] : \dot{\boldsymbol{\alpha}} \, dv \tag{49}$$

which from (42) can be rewritten as

$$\dot{W}(t) \leq -D(t) + \int_\Omega \Big[-\boldsymbol{A}^r + \frac{1}{m} \big(\boldsymbol{B}_* + \nabla h(\boldsymbol{\alpha}_*) + \boldsymbol{A}^d_* + \boldsymbol{A}^r_* \big) \Big] : \dot{\boldsymbol{\alpha}} \, dv. \tag{50}$$

where

$$\boldsymbol{A}^r_* = (\boldsymbol{A}^r_{*,1}, 0), \;\; \boldsymbol{A}^d_* = \mathbb{K}^T : (m\boldsymbol{\sigma}^E + \boldsymbol{\rho}_*) - \boldsymbol{B}_* - \nabla h(\boldsymbol{\alpha}_*) - \boldsymbol{A}^r_* \in \mathcal{C}.$$

Since $\boldsymbol{A}^d_* \in \mathcal{C}$ and $\dot{\boldsymbol{\alpha}} \in \partial \mathcal{C}(\boldsymbol{A}^d)$, relation (4) gives

$$(\boldsymbol{A}^d - \boldsymbol{A}^d_*) : \dot{\boldsymbol{\alpha}} \geq 0. \tag{51}$$

Similarly, since $\boldsymbol{A}^r \in \partial\mathcal{T}(\boldsymbol{\alpha})$ and $\boldsymbol{\alpha} \in \mathcal{T}$, relation (4) implies that $0 \geq \boldsymbol{A}^r(\boldsymbol{x},t) : (\boldsymbol{\alpha}(\boldsymbol{x},t') - \boldsymbol{\alpha}(\boldsymbol{x},t))$ for all t'. Applying that last inequality with $t' = t - \delta t$ and taking the limit $\delta t \longrightarrow 0^+$, we obtain

$$\boldsymbol{A}^r : \dot{\boldsymbol{\alpha}} \geq 0. \tag{52}$$

Combining (51) and (52) with (50) yields

$$\dot{W}(t) \leq -D(t) + \frac{1}{m}\int_\Omega \left[\boldsymbol{B}_* + \nabla h(\boldsymbol{\alpha}_*) + \boldsymbol{A}^d + \boldsymbol{A}^r_*\right] : \dot{\boldsymbol{\alpha}}\, dv$$

i.e.

$$\dot{W}(t) \leq \frac{1-m}{m} D(t) + \frac{1}{m}\int_\Omega \left[\boldsymbol{B}_* + \nabla h(\boldsymbol{\alpha}_*) + \boldsymbol{A}^r_*\right] : \dot{\boldsymbol{\alpha}}\, dv. \tag{53}$$

4.1.3. Bound on the dissipated energy

Integrating (53) with respect to time on $[T,t]$ gives

$$(m-1)\int_T^t D(t)\, dt \leq m(W(T) - W(t)) + \int_\Omega (\boldsymbol{B}_* + \nabla h(\boldsymbol{\alpha}_*) + \boldsymbol{A}^r_*) : (\boldsymbol{\alpha}(\boldsymbol{x},t)) - \boldsymbol{\alpha}(\boldsymbol{x},T))\, dv \tag{54}$$

where the properties $\dot{\boldsymbol{A}}^r_* = \dot{\boldsymbol{\alpha}}_* = \dot{\boldsymbol{B}}_* = 0$ have been used. Since $\boldsymbol{B}_* \in \partial f(\boldsymbol{\alpha}_*)$ and f is convex, we have $\boldsymbol{B}_* : (\boldsymbol{\alpha} - \boldsymbol{\alpha}_*) \leq f(\boldsymbol{\alpha}) - f(\boldsymbol{\alpha}_*)$. Hence

$$\begin{aligned} \boldsymbol{B}_* : (\boldsymbol{\alpha}(\boldsymbol{x},t) - \boldsymbol{\alpha}(\boldsymbol{x},T)) \quad &= \boldsymbol{B}_* : (\boldsymbol{\alpha}(\boldsymbol{x},t) - \boldsymbol{\alpha}_*(\boldsymbol{x})) + \boldsymbol{B}_* : (\boldsymbol{\alpha}_*(\boldsymbol{x}) - \boldsymbol{\alpha}(\boldsymbol{x},T)) \\ &\leq f(\boldsymbol{\alpha}(\boldsymbol{x},t)) - f(\boldsymbol{\alpha}_*(\boldsymbol{x})) + \boldsymbol{B}_* : (\boldsymbol{\alpha}_*(\boldsymbol{x}) - \boldsymbol{\alpha}(\boldsymbol{x},T)). \end{aligned}$$

It follows that

$$\begin{aligned} (m-1)\int_T^t D(t)\, dt \leq \quad & m(W(T) - W(t)) + \int_\Omega f(\boldsymbol{\alpha}(\boldsymbol{x},t)) - f(\boldsymbol{\alpha}_*(\boldsymbol{x}))\, dv \\ & + \int_\Omega \boldsymbol{B}_* : (\boldsymbol{\alpha}_*(\boldsymbol{x}) - \boldsymbol{\alpha}(\boldsymbol{x},T))\, dv \\ & + \int_\Omega (\boldsymbol{A}^r_* + \nabla h(\boldsymbol{\alpha}_*)) : (\boldsymbol{\alpha}(\boldsymbol{x},t) - \boldsymbol{\alpha}(\boldsymbol{x},T))\, dv. \end{aligned} \tag{55}$$

Recalling that $\mathbb{L}$ is positive definite and $h \geq 0$, the definition (44) of $W(t)$ implies that $W(t) \geq \int_\Omega f(\boldsymbol{\alpha}(\boldsymbol{x},t))dv$. Since $m > 1$ and $f \geq 0$, we have a fortiori $mW(t) \geq \int_\Omega f(\boldsymbol{\alpha}(\boldsymbol{x},t))dv$. Hence (55) yields

$$\begin{aligned} (m-1)\int_T^t D(t)\, dt \leq \quad & mW(T) + \int_\Omega \left[-f(\boldsymbol{\alpha}_*(\boldsymbol{x})) + \boldsymbol{B}_* : (\boldsymbol{\alpha}_*(\boldsymbol{x}) - \boldsymbol{\alpha}(\boldsymbol{x},T))\right] dv \\ & + \int_\Omega (\boldsymbol{A}^r_* + \nabla h(\boldsymbol{\alpha}_*)) : (\boldsymbol{\alpha}(\boldsymbol{x},t) - \boldsymbol{\alpha}(\boldsymbol{x},T))\, dv. \end{aligned} \tag{56}$$

The last integral in the right hand side of (56) can be bounded independently of time t. Recall indeed that

$$\big(\boldsymbol{A}^r_* + \nabla h(\boldsymbol{\alpha}_*)\big) : \big(\boldsymbol{\alpha}(\boldsymbol{x},t) - \boldsymbol{\alpha}(\boldsymbol{x},T)\big) = \big(\boldsymbol{A}^r_{1,*} + h'(\boldsymbol{\alpha}_{1,*})\big) : \big(\boldsymbol{\alpha}_1(\boldsymbol{x},t) - \boldsymbol{\alpha}_1(\boldsymbol{x},T)\big).$$

Since $\mathcal{T}_1$ is bounded, there exists a constant $C > 0$ such that $\|\boldsymbol{\alpha}_1\| \leq C$ for all $\boldsymbol{\alpha}_1 \in \mathcal{T}_1$. Using the Cauchy-Schwarz inequality, we obtain

$$\begin{aligned} \|(\boldsymbol{A}^r_{1,*} + h'(\boldsymbol{\alpha}_{1,*})) : (\boldsymbol{\alpha}_1(\boldsymbol{x},t) - \boldsymbol{\alpha}_1(\boldsymbol{x},T))\| &\leq \|\boldsymbol{A}^r_{1,*} + h'(\boldsymbol{\alpha}_{1,*})\|.\|\boldsymbol{\alpha}_1(\boldsymbol{x},t) - \boldsymbol{\alpha}_1(\boldsymbol{x},T)\| \\ &\leq 2C\|\boldsymbol{A}^r_{1,*} + h'(\boldsymbol{\alpha}_{1,*})\|. \end{aligned}$$

Therefore

$$\begin{aligned} (m-1)\int_T^t D(t)\,dt \leq \;& mW(T) + \int_\Omega \left[-f(\boldsymbol{\alpha}_*(\boldsymbol{x})) + \boldsymbol{B}_* : (\boldsymbol{\alpha}_*(\boldsymbol{x}) - \boldsymbol{\alpha}(\boldsymbol{x},T))\right] dv \\ &+2C\int_\Omega \|\boldsymbol{A}^r_{1,*} + h'(\boldsymbol{\alpha}_{1,*})\|\,dv. \end{aligned} \tag{57}$$

The right-hand side of (57) is independent of t and consequently the dissipated energy $\int_T^t D(t)\,dt$ is bounded as $t \to +\infty$. This concludes the proof that Condition 3 is a sufficient condition for shakedown to occur, whatever the initial state.

4.2. Static shakedown theorem

Condition 3 can actually be rewritten in a form that is more convenient for practical applications. Let indeed $\boldsymbol{\rho}_*$, $\boldsymbol{\alpha}_*$ and $\boldsymbol{B}_* = (\boldsymbol{B}_{1,*}, \boldsymbol{B}_{2,*})$ be given fields in $\mathcal{K}^0_\sigma$, $\mathcal{T}$ and $\partial f(\boldsymbol{\alpha}_*)$, respectively. Those fields satisfy (42) if and only we can find $\boldsymbol{A}^r_{1,*} \in \mathrm{dev}(\mathbb{R}^{3\times 3}_s)$ such that

$$m\mathbb{K}^T : \boldsymbol{\sigma}^E + (\mathbb{K}^T_1 : \boldsymbol{\rho}_*, \mathbb{K}^T_2 : \boldsymbol{\rho}_*) - (h'(\boldsymbol{\alpha}_*), 0) - (\boldsymbol{B}_{1,*}, \boldsymbol{B}_{2,*}) - (\boldsymbol{A}^r_{1,*}, 0) \in \mathcal{C}$$

i.e.

$$m\mathbb{K}^T : \boldsymbol{\sigma}^E + \big(\mathbb{K}^T_1 : \boldsymbol{\rho}_* - \boldsymbol{B}_{1,*} - h'(\boldsymbol{\alpha}_*) - \boldsymbol{A}^r_{1,*}, \mathbb{K}^T_2 : \boldsymbol{\rho}_* - \boldsymbol{B}_{2,*}\big) \in \mathcal{C}. \tag{58}$$

Since $\boldsymbol{A}^r_{1,*}$ is free from any constraint, Eq.(58)is satisfied for some $\boldsymbol{A}^r_{1,*}$ if and only if

$$m\mathbb{K}^T : \boldsymbol{\sigma}^E - (\boldsymbol{B}_1, \boldsymbol{B}_{2,*} - \mathbb{K}^T_2 : \boldsymbol{\rho}_*) \in \mathcal{C} \tag{59}$$

for some time-independent $\boldsymbol{B}_1 \in \mathrm{dev}(\mathbb{R}^{3\times 3}_s)$. Let

$$\mathcal{B}_2 = \{\boldsymbol{B}_2 | (\boldsymbol{B}_1, \boldsymbol{B}_2) \in \partial f(\boldsymbol{\alpha}), \boldsymbol{\alpha} \in \mathcal{T}\}.$$

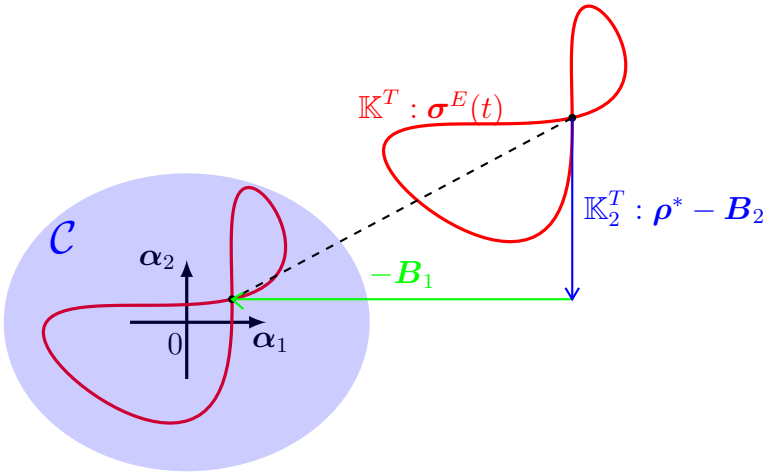

Figure 2: Geometric interpretation of the shakedown condition.

In the particular case where f is differentiable, $\mathcal{B}_2$ is the set of values taken by the partial derivative $\partial f/\partial \boldsymbol{\alpha}_2$ as $\boldsymbol{\alpha}$ varies in $\mathcal{T}$. Eq. (59) can equivalently be rewritten as

$$m\mathbb{K}^T : \boldsymbol{\sigma}^E - (\boldsymbol{B}_1, \boldsymbol{B}_2 - \mathbb{K}_2^T : \boldsymbol{\rho}_*) \in \mathcal{C} \tag{60}$$

for some $(\boldsymbol{B}_1, \boldsymbol{B}_2) \in \mathrm{dev}(\mathbb{R}_s^{3\times 3}) \times \mathcal{B}_2$. We can thus state the following theorem:

Static shakedown theorem. *If there exists $m > 1$, $T \geq 0$ and time-independent fields $\boldsymbol{\rho}_* \in \mathcal{K}_\sigma^0$, $\boldsymbol{B} \in \mathrm{dev}(\mathbb{R}_s^{3\times 3}) \times \mathcal{B}_2$ such that Eq.(60) is satisfied for all $\boldsymbol{x} \in \Omega$ and $t \geq T$ then shakedown occurs, whatever the initial condition is.*

For simplicity, from here onward we restrict our attention to cyclic loadings: the function $\boldsymbol{\sigma}^E$ is assumed to be periodic in time with a period T. A geometric interpretation of the shakedown condition is supplied in Fig. 2. Consider a given location $\boldsymbol{x}$. As t varies, $\mathbb{K}^T : \boldsymbol{\sigma}^E(\boldsymbol{x}, t)$ describes a closed curve $\Gamma(\boldsymbol{x})$ in the product space $\mathrm{dev}(\mathbb{R}_s^{3\times 3}) \times \mathrm{dev}(\mathbb{R}_s^{3\times 3})$. The obtained theorem states that shakedown occurs if, up to a translation $\boldsymbol{B}(x) = (\boldsymbol{B}_1(\boldsymbol{x}), \boldsymbol{B}_2(\boldsymbol{x}))$, the curve $\Gamma(\boldsymbol{x})$ is enclosed in the elasticity domain $\mathcal{C}$. The translation component $\boldsymbol{B}_1$ can be chosen arbitrarily but $\boldsymbol{B}_2$ needs to be of the form $\boldsymbol{B}_2 = \mathbb{K}_2^T : \boldsymbol{\rho}^* - \boldsymbol{B}_2^*$ for some $\boldsymbol{\rho}^* \in \mathcal{K}_\sigma^0$ and $\boldsymbol{B}_2^* \in \mathcal{B}_2$. Since differential constraints are involved in the definition of $\boldsymbol{\rho}^*$, the values of $\boldsymbol{B}_2$ at two given locations $\boldsymbol{x}$ and $\boldsymbol{x}'$ cannot *a priori* be chosen independently.

The static shakedown theorem motivates the definition of the static safety coef-

ficient m_S by

$$m_S = \sup_{\substack{(m,\boldsymbol{\rho}_*,\boldsymbol{B}_1,\boldsymbol{B}_2)\in\mathbb{R}\times\mathcal{K}^0_\sigma\times\operatorname{dev}\mathbb{R}^{3\times3}_s\times\mathcal{B}_2 \\ \text{verifying (60) for all } \boldsymbol{x},t}} m. \tag{61}$$

If $m_S > 1$ then shakedown occurs (for all initial states) as a consequence of the shakedown theorem stated above. The larger m_S is, the safer the structure is with respect to fatigue.

4.3. Applications to some material models

4.3.1. Model of Auricchio et al. (2007)

As a first example, consider the material model of Auricchio et al. (2007) as presented previously in Sect. 2.1. Consider a given location $\boldsymbol{x}$ and a given m. Using the expression (20) of the elasticity domain, shakedown condition (60) consists in checking whether some $(\boldsymbol{B}_1,\boldsymbol{B}_2)\in\operatorname{dev}(\mathbb{R}^{3\times3}_s)\times\mathcal{B}_2$ can be found such that

$$\sup_t \|m\boldsymbol{s}^E(\boldsymbol{x},t)-\boldsymbol{B}_1\|+\kappa\|\boldsymbol{B}_2\|\le R. \tag{62}$$

In (62), $\boldsymbol{s}^E$ is the deviatoric part of $\boldsymbol{\sigma}^E$. Observe that the stress field $\boldsymbol{\rho}_*$ in (60) disappears because $\mathbb{K}_2=0$ for the model of Auricchio et al. (2007). Some $(\boldsymbol{B}_1,\boldsymbol{B}_2)\in\operatorname{dev}(\mathbb{R}^{3\times3}_s)\times\mathcal{B}_2$ satisfying (62) can be found if

$$\min_{\boldsymbol{B}_1\in\operatorname{dev}(\mathbb{R}^{3\times3}_s)}\min_{\boldsymbol{B}_2\in\mathcal{B}_2}\sup_t\left[\|m\boldsymbol{s}^E(\boldsymbol{x},t)-\boldsymbol{B}_1\|+\kappa\|\boldsymbol{B}_2\|\right]\le R$$

i.e.

$$\min_{\boldsymbol{B}_1\in\operatorname{dev}(\mathbb{R}^{3\times3}_s)}\sup_t\|m\boldsymbol{s}^E(\boldsymbol{x},t)-\boldsymbol{B}_1\|+\min_{\boldsymbol{B}_2\in\mathcal{B}_2}\kappa\|\boldsymbol{B}_2\|\le R. \tag{63}$$

Evaluating the minimum with respect to $\boldsymbol{B}_2$ in (63) requires the expression of the set $\mathcal{B}_2$. For the model of Auricchio et al. (2007), it can be calculated (see Appendix A) that

$$\mathcal{B}_2=\begin{cases}\operatorname{dev}(\mathbb{R}^{3\times3}_s) & \text{if } H_2>0,\\ \{\boldsymbol{\tau}:\operatorname{tr}\boldsymbol{\tau}=0,\|\boldsymbol{\tau}\|\le\tau_M\} & \text{if } H_2=0.\end{cases} \tag{64}$$

It follows that $\min_{\boldsymbol{B}_2\in\mathcal{B}_2}\kappa\|\boldsymbol{B}_2\|=0$, so that (63) reduces to

$$m\gamma(\boldsymbol{x})\le R \tag{65}$$

where

$$\gamma(\boldsymbol{x})=\min_{\boldsymbol{B}_1\in\operatorname{dev}(\mathbb{R}^{3\times3}_s)}\sup_t\|\boldsymbol{s}^E(\boldsymbol{x},t)-\boldsymbol{B}_1\| \tag{66}$$

can be interpreted as the radius of the curve $t \mapsto \boldsymbol{s}^E(\boldsymbol{x},t)$, i.e. the radius of the smallest hypersphere enclosing $t \mapsto \boldsymbol{s}^E(\boldsymbol{x},t)$ in the space of deviatoric stress. The conclusion is that condition (62) can be satisfied for all $\boldsymbol{x}$ if and only if $m \leq R/\gamma(\boldsymbol{x})$ for all $\boldsymbol{x}$, hence

$$m_S = \frac{R}{\sup_{\boldsymbol{x}} \gamma(\boldsymbol{x})}. \tag{67}$$

Recall that shakedown occurs if $m_S > 1$. The obtained shakedown condition thus reduces to a restriction on the radius of the curve $t \mapsto \boldsymbol{s}^E(\boldsymbol{x},t)$.

Remark: It can be verified that (67) remains valid if expression (21) of the elasticity domain is adopted instead of (20).

4.3.2. Model of Barrera et al. (2014)

Let us now consider the model of Barrera et al. (2014) as formulated by Eqs (28) and (32). Recalling that $\mathbb{K}_1 = -a\mathbb{K}$ and $\mathbb{K}_2 = -(1+a)\mathbb{K}$ for that model, we have

$$m\mathbb{K}^T : \boldsymbol{\sigma}^E + (0, \mathbb{K}_2^T : \boldsymbol{\rho}_*) = -\left(am\boldsymbol{s}^E, (1+a)(m\boldsymbol{s}^E + \boldsymbol{s}_*)\right)$$

where $\boldsymbol{s}_*$ is the deviatoric part of $\boldsymbol{\rho}_*$. Using expression (32) of the elasticity domain, the shakedown condition (60) to be satisfied at any given $\boldsymbol{x}$ becomes

$$\sup_t \max\left\{\|m\boldsymbol{s}^E(\boldsymbol{x},t) + (1+a)\boldsymbol{s}_* - \boldsymbol{B}_1 + \boldsymbol{B}_2\|, \kappa\|ma\boldsymbol{s}^E(\boldsymbol{x},t) + \boldsymbol{B}_1\|\right\} \leq R \tag{68}$$

for some $(\boldsymbol{\rho}_*, \boldsymbol{B}_1, \boldsymbol{B}_2) \in \mathcal{K}_\sigma^0 \times \mathrm{dev}(\mathbb{R}_s^{3\times 3}) \times \mathcal{B}_2$. For the model of Barrera et al. (2014), the function f is given by (29) and is differentiable. We have $\mathcal{B}_2 = \{H(\boldsymbol{\alpha}_1 + \boldsymbol{\alpha}_2), \boldsymbol{\alpha}_1 \in \mathcal{T}_1, \boldsymbol{\alpha}_2 \in \mathrm{dev}(\mathbb{R}_s^{3\times 3})\}$ where $\mathcal{T}_1$ is defined as in (14). Hence

$$\mathcal{B}_2 = \begin{cases} \mathrm{dev}(\mathbb{R}_s^{3\times 3}) & \text{if } H > 0, \\ 0 & \text{if } H = 0. \end{cases} \tag{69}$$

Let us first consider the case $H > 0$ and set $\boldsymbol{B}_2' = (1+a)\boldsymbol{s}_* - \boldsymbol{B}_1 + \boldsymbol{B}_2$. For any given $\boldsymbol{B}_1$ and $\boldsymbol{s}_*$, the term $\boldsymbol{B}_2'$ can take any value in $\mathrm{dev}(\mathbb{R}_s^{3\times 3})$ as $\boldsymbol{B}_2$ varies in $\mathcal{B}_2 = \mathrm{dev}(\mathbb{R}_s^{3\times 3})$. As a consequence, the condition for (68) to be satisfied for some $(\boldsymbol{\rho}_*, \boldsymbol{B}_1, \boldsymbol{B}_2) \in \mathcal{K}_\sigma^0 \times \mathrm{dev}(\mathbb{R}_s^{3\times 3}) \times \mathcal{B}_2$ is simply that

$$\inf_{\boldsymbol{B}_1, \boldsymbol{B}_2' \in \mathrm{dev}(\mathbb{R}_s^{3\times 3})} \sup_t \max\left\{\|m\boldsymbol{s}^E(\boldsymbol{x},t) + \boldsymbol{B}_2'\|, \kappa\|ma\boldsymbol{s}^E(\boldsymbol{x},t) + \boldsymbol{B}_1\|\right\} \leq R. \tag{70}$$

Noting that the variables $\boldsymbol{B}_1$ and $\boldsymbol{B}_2'$ in (70) are uncoupled, Eq. (70) is equivalent to

$$\begin{cases} \inf\limits_{\boldsymbol{B}_1 \in \mathrm{dev}(\mathbb{R}_s^{3\times 3})} \sup\limits_t \kappa\|ma\boldsymbol{s}^E(\boldsymbol{x},t) + \boldsymbol{B}_1\| \} & \leq R, \\ \inf\limits_{\boldsymbol{B}_2' \in \mathrm{dev}(\mathbb{R}_s^{3\times 3})} \sup\limits_t \|m\boldsymbol{s}^E(\boldsymbol{x},t) + \boldsymbol{B}_2'\| & \leq R, \end{cases} \tag{71}$$

i.e.

$$a\kappa m\gamma(\boldsymbol{x}) \leq R \text{ and } m\gamma(\boldsymbol{x}) \leq R \tag{72}$$

where $\gamma(\boldsymbol{x})$ is defined as in (66). From (72) we obtain

$$m_S = \frac{R/\max(1, a\kappa)}{\sup_{\boldsymbol{x}} \gamma(\boldsymbol{x})}. \tag{73}$$

The obtained shakedown condition again reduces to a restriction on the radius of the curve $t \mapsto \boldsymbol{s}^E(\boldsymbol{x}, t)$.

In the case $H = 0$, we have $\mathcal{B}_2 = 0$ from (69) so that shakedown condition (68) becomes

$$\sup_t \max\{\|m\boldsymbol{s}^E(\boldsymbol{x}, t) + (1 + a)\boldsymbol{s}_* - \boldsymbol{B}_1\|, \kappa\|ma\boldsymbol{s}^E(\boldsymbol{x}, t) - \boldsymbol{B}_1\|\} \leq R \tag{74}$$

for some $(\boldsymbol{B}_1, \boldsymbol{\rho}_*) \in \text{dev}(\mathbb{R}^{3\times3}_s) \times \mathcal{K}^0_\sigma$. Hence

$$m_S = \sup_{\substack{(m, \boldsymbol{\rho}_*, \boldsymbol{B}_1) \in \mathbb{R} \times \mathcal{K}^0_\sigma \times \text{dev}\,\mathbb{R}^{3\times3}_s \\ \text{verifying (74) for all } \boldsymbol{x}, t}} m \tag{75}$$

It does not seem possible to obtain an explicit expression of m_S in (75), i.e. to solve the optimization problem (75) explicitly. However, lower bounds on m_S can be obtained by constructing particular values of $(m, \boldsymbol{\rho}_*, \boldsymbol{B}_1, \boldsymbol{B}_2)$ (possibly through numerical procedure) satisfying (60). Upper bounds on m_S are next considered in Section 5.

.

5. Kinematic approach

5.1. Upper bounds on m_S

Upper bounds on m_S are useful in situations where the coefficient m_S in (76) cannot be calculated exactly. Such bounds can be obtained by convex duality, as notably used by Nguyen (2003) in the context of plasticity. Let $\mathcal{A}$ be the convex set formed by uplets $(m, \boldsymbol{\rho}_*, \boldsymbol{B}, \tilde{\boldsymbol{\Sigma}})$ such that $\boldsymbol{\rho}_*(\boldsymbol{x}) \in \mathcal{K}^0_\sigma$ is a time-independent self-equilibrated stress field, $\boldsymbol{B}(\boldsymbol{x})$ is time independent with values in $\text{dev}(\mathbb{R}^{3\times3}_s) \times \mathcal{B}_2$ and $\tilde{\boldsymbol{\Sigma}}(\boldsymbol{x}, t) \in \mathcal{C}$ for all $(\boldsymbol{x}, t)$. From (61) we have

$$m_S = \sup_{\substack{(m, \boldsymbol{\rho}^*, \boldsymbol{B}, \tilde{\boldsymbol{\Sigma}}) \in \mathcal{A}, \\ m\mathbb{K}^T : \boldsymbol{\sigma}^E + (0, \mathbb{K}^T_2 : \boldsymbol{\rho}_*) - \boldsymbol{B} = \tilde{\boldsymbol{\Sigma}}}} m. \tag{76}$$

The right-hand side of (76) is a constrained maximization problem over the set $\mathcal{A}$. We note that $\mathcal{B}_2$ and consequently $\mathcal{A}$ are convex in situations of interest. Let $\mathcal{L}$ be the lagrangian corresponding to (76), i.e.

$$\begin{aligned}\mathcal{L}(m, \boldsymbol{\rho}_*, \boldsymbol{B}, \tilde{\boldsymbol{\Sigma}}; \boldsymbol{d}) &= m \\ &+ \int_\Omega \int_0^T \left[\boldsymbol{d}(\boldsymbol{x}, t) : \left(\tilde{\boldsymbol{\Sigma}}(\boldsymbol{x}, t) - m\mathbb{K}^T : \boldsymbol{\sigma}^E(\boldsymbol{x}, t) - (0, \mathbb{K}_2^T : \boldsymbol{\rho}_*(\boldsymbol{x})) + \boldsymbol{B}(\boldsymbol{x}) \right) \right] dvdt\end{aligned} \tag{77}$$

where $\boldsymbol{d}(\boldsymbol{x}, t) \in \mathrm{dev}(\mathbb{R}_s^{3\times 3})^2$ is a Lagrange multiplier associated to the constraint $m\mathbb{K}^T : \boldsymbol{\sigma}^E + (0, \mathbb{K}_2^T : \boldsymbol{\rho}_*) - \boldsymbol{B} = \tilde{\boldsymbol{\Sigma}}$. We have

$$m_S = \sup_{(m, \boldsymbol{\rho}_*, \boldsymbol{B}, \tilde{\boldsymbol{\Sigma}}) \in \mathcal{A}} \inf_{\boldsymbol{d}} \mathcal{L}(m, \boldsymbol{\rho}_*, \boldsymbol{B}, \tilde{\boldsymbol{\Sigma}}; \boldsymbol{d}).$$

The min-max inequality

$$\sup_{(m, \boldsymbol{\rho}_*, \boldsymbol{B}, \tilde{\boldsymbol{\Sigma}}) \in \mathcal{A}} \inf_{\boldsymbol{d}} \mathcal{L} \leq \inf_{\boldsymbol{d}} \sup_{(m, \boldsymbol{\rho}_*, \boldsymbol{B}, \tilde{\boldsymbol{\Sigma}}) \in \mathcal{A}} \mathcal{L} \tag{78}$$

gives

$$m_S \leq m_K \tag{79}$$

where

$$m_K = \inf_{\boldsymbol{d}} \sup_{(m, \boldsymbol{\rho}_*, \boldsymbol{B}, \tilde{\boldsymbol{\Sigma}}) \in \mathcal{A}} \mathcal{L}(m, \boldsymbol{\rho}_*, \boldsymbol{B}, \tilde{\boldsymbol{\Sigma}}; \boldsymbol{d}).$$

We now proceed to rewrite the coefficient m_K in a more explicit form. For a given $\boldsymbol{d} = (\boldsymbol{d}_1, \boldsymbol{d}_2)$, expression (77) of $\mathcal{L}$ yields

$$\sup_{(m, \boldsymbol{\rho}_*, \boldsymbol{B}, \tilde{\boldsymbol{\Sigma}}) \in \mathcal{A}} \mathcal{L}(m, \boldsymbol{\rho}_*, \boldsymbol{B}, \tilde{\boldsymbol{\Sigma}}; \boldsymbol{d}) = S_1 + S_2 + S_3 + S_4 \tag{80}$$

where

$$\begin{aligned} S_1 &= \sup_m m \left(1 - \int_\Omega \int_0^T \boldsymbol{\sigma}^E(\boldsymbol{x}, t) : \mathbb{K} : \boldsymbol{d}(\boldsymbol{x}, t) dvdt \right), \\ S_2 &= \sup_{\tilde{\boldsymbol{\Sigma}} \in \mathcal{C}} \int_\Omega \int_0^T \boldsymbol{d}(\boldsymbol{x}, t) : \tilde{\boldsymbol{\Sigma}}(\boldsymbol{x}, t) dvdt, \\ S_3 &= \sup_{\boldsymbol{\rho}_* \in \mathcal{K}_\sigma^0} - \int_\Omega \boldsymbol{\rho}_*(\boldsymbol{x}) : \mathbb{K}_2 : \boldsymbol{E}_2(\boldsymbol{x}) dvdt, \\ S_4 &= \sup_{\boldsymbol{B} \in \mathrm{dev}(\mathbb{R}_s^{3\times 3}) \times \mathcal{B}_2} \int_\Omega \boldsymbol{E}(\boldsymbol{x}) : \boldsymbol{B}(\boldsymbol{x}) dv \end{aligned} \tag{81}$$

and $\boldsymbol{E} = (\boldsymbol{E}_1, \boldsymbol{E}_2)$ with $\boldsymbol{E}_i(\boldsymbol{x}) = \int_0^T \boldsymbol{d}_i(\boldsymbol{x}, t)dt$. Let us examine each maximization problem in (81). Clearly

$$S_1 = \begin{cases} 0 & \text{if } \int_\Omega \int_0^T \boldsymbol{\sigma}^E : \mathbb{K} : \boldsymbol{d}\, dvdt = 1, \\ \infty & \text{otherwise,} \end{cases}$$

and we have

$$S_2 = \int_\Omega \int_0^T \mathcal{D}(\boldsymbol{d}(\boldsymbol{x}, t))dvdt$$

where $\mathcal{D}$ is the function defined by

$$\mathcal{D}(\boldsymbol{d}) = \sup_{\Sigma \in \mathcal{C}} \Sigma : \boldsymbol{d} \tag{82}$$

for any $\boldsymbol{d} \in \operatorname{dev} \mathbb{R}^{3\times 3}_s$. We now show that

$$S_3 = \begin{cases} 0 & \text{if } \mathbb{K}_2 : \boldsymbol{E}_2 \in \mathcal{K}^0_\epsilon, \\ \infty & \text{otherwise.} \end{cases} \tag{83}$$

Let indeed $\boldsymbol{\rho}^r$ and $\boldsymbol{\varepsilon}^r$ be the residual stress and strain fields associated with the strain field $\mathbb{K}_2 : \boldsymbol{E}_2$, i.e. the solution to the elasticity problem

$$\boldsymbol{\rho}^r \in \mathcal{K}^0_\sigma,\ \boldsymbol{\varepsilon}^r \in \mathcal{K}^0_\epsilon,\ \boldsymbol{\varepsilon}^r = \mathbb{L}^{-1} : \boldsymbol{\rho}^r + \mathbb{K}_2 : \boldsymbol{E}_2. \tag{84}$$

It follows from (84) and (40) that

$$0 = \int_\Omega \boldsymbol{\rho}^* : \mathbb{L}^{-1} : \boldsymbol{\rho}^r + \int_\Omega \boldsymbol{\rho}^* : \mathbb{K}_2 : \boldsymbol{E}_2 \tag{85}$$

for any $\boldsymbol{\rho}^* \in \mathcal{K}^0_\sigma$. Choosing $\boldsymbol{\rho}^* = x\boldsymbol{\rho}^r$ in (85) and taking the limit $x \to \infty$ shows that

$$\sup_{\boldsymbol{\rho}^* \in \mathcal{K}^0_\sigma} -\int_\Omega \boldsymbol{\rho}^* : \mathbb{K}_2 : \boldsymbol{E}_2 dv = \infty \text{ if } \boldsymbol{\rho}^r \neq 0.$$

On the other hand, it follows directly from (84) that

$$\sup_{\boldsymbol{\rho}^* \in \mathcal{K}^0_\sigma} -\int_\Omega \boldsymbol{\rho}^* : \mathbb{K}_2 : \boldsymbol{E}_2 dv = 0 \text{ if } \boldsymbol{\rho}^r = 0.$$

The condition $\boldsymbol{\rho}^r = 0$ means that $\mathbb{K}_2 : \boldsymbol{E}_2 \in \mathcal{K}^0_\epsilon$. This completes the proof of (83).

It now remains to evaluate the term S_4 in (81). Writing $\boldsymbol{B} = (\boldsymbol{B}_1, \boldsymbol{B}_2)$ with $\boldsymbol{B}_1 \in \mathrm{dev}(\mathbb{R}^{3\times 3}_s)$ and $\boldsymbol{B}_2 \in \mathcal{B}_2$, we have

$$S_4 = \sup_{\boldsymbol{B}_1 \in \mathrm{dev}(\mathbb{R}^{3\times 3}_s)} \int_\Omega \boldsymbol{E}_1(\boldsymbol{x}) : \boldsymbol{B}_1(\boldsymbol{x}) dv + \sup_{\boldsymbol{B}_2 \in \mathcal{B}_2} \int_\Omega \boldsymbol{E}_2(\boldsymbol{x}) : \boldsymbol{B}_2(\boldsymbol{x}) dv.$$

It can be observed that

$$\sup_{\boldsymbol{B}_1 \in \mathrm{dev}(\mathbb{R}^{3\times 3}_s)} \int_\Omega \boldsymbol{E}_1(\boldsymbol{x}) : \boldsymbol{B}_1(\boldsymbol{x}) dv = \begin{cases} 0 & \text{if } \boldsymbol{E}_1(\boldsymbol{x}) = 0 \text{ for all } \boldsymbol{x}, \\ \infty & \text{otherwise.} \end{cases}$$

We have

$$\sup_{\boldsymbol{B}_2 \in \mathcal{B}_2} \int_\Omega \boldsymbol{E}_2(\boldsymbol{x}) : \boldsymbol{B}_2(\boldsymbol{x}) dv = \int_\Omega \mathcal{P}(\boldsymbol{E}_2(\boldsymbol{x})) dv$$

where $\mathcal{P}$ is the function defined for any $\boldsymbol{E} \in \mathrm{dev}(\mathbb{R}^{3\times 3}_s)$ by

$$\mathcal{P}(\boldsymbol{E}) = \sup_{\boldsymbol{B}_2 \in \mathcal{B}_2} \boldsymbol{B}_2 : \boldsymbol{E}. \tag{86}$$

Let us collect the results established so far: If $\boldsymbol{d}$ satisfies the conditions

$$\int_0^T \int_\Omega \boldsymbol{\sigma}^E : \mathbb{K} : \boldsymbol{d}\, dv dt = 1, \int_0^T \boldsymbol{d}_1 dt = 0 \text{ and } \mathbb{K}_2 : \left(\int_0^T \boldsymbol{d}_2 dt \right) \in \mathcal{K}^0_\epsilon \tag{87}$$

then we have

$$\sup_{(m, \boldsymbol{\rho}^*, \boldsymbol{B}, \tilde{\boldsymbol{\Sigma}}) \in \mathcal{A}} \mathcal{L}(m, \boldsymbol{\rho}^*, \boldsymbol{B}, \tilde{\boldsymbol{\Sigma}}; \boldsymbol{d}) = \int_\Omega \int_0^T \mathcal{D}(\boldsymbol{d}(\boldsymbol{x}, t)) dv dt + \int_\Omega \mathcal{P}(\boldsymbol{E}_2(\boldsymbol{x})) dv.$$

If $\boldsymbol{d}$ does not satisfy (87) then

$$\sup_{(m, \boldsymbol{\rho}^*, \boldsymbol{B}, \tilde{\boldsymbol{\Sigma}}) \in \mathcal{A}} \mathcal{L}(m, \boldsymbol{\rho}^*, \boldsymbol{B}, \tilde{\boldsymbol{\Sigma}}; \boldsymbol{d}) = +\infty$$

Hence

$$m_K = \inf_{\boldsymbol{d}} \int_\Omega \int_0^T \mathcal{D}(\boldsymbol{d}(\boldsymbol{x}, t)) dv dt + \int_\Omega \mathcal{P}(\boldsymbol{E}_2(\boldsymbol{x})) dv \tag{88}$$

where the infimum is taken over histories $\boldsymbol{d}$ that satisfy (87). In practice, an upper bound m_K^+ on m_K (and therefore on m_S) can be obtained by constructing histories $\boldsymbol{d}$ satisfying the requirements (87).

5.2. Kinematic shakedown theorem

Consider the situation where there exists $\boldsymbol{d}$ satisfying (87) and

$$\int_\Omega \int_0^T \mathcal{D}(\boldsymbol{d}(\boldsymbol{x},t))dvdt + \int_\Omega \mathcal{P}(\boldsymbol{E}_2(\boldsymbol{x}))dv < 1.$$

Eq (88) implies that $m_K < 1$. It follows from (79) that $m_S < 1$, i.e. that shakedown is not guaranteed. We can thus formulate the following

Kinematic shakedown theorem. *If there exists $\boldsymbol{d}$ satisfying Eq. (87) and such that $\int_\Omega \int_0^T \mathcal{D}(\boldsymbol{d}(\boldsymbol{x},t))dvdt + \int_\Omega \mathcal{P}(\boldsymbol{E}_2(\boldsymbol{x}))dv < 1$ then shakedown is not ensured for all initial states.*

5.3. Applications

5.3.1. Model of Auricchio et al. (2007)

From the expression (20) of the elasticity domain, it can be calculated that the function $\mathcal{D}$ introduced in (82) is equal to

$$\mathcal{D}(\boldsymbol{d}) = R \max\left(\|\boldsymbol{d}_1\|, \frac{\|\boldsymbol{d}_2\|}{\kappa} \right).$$

It is necessary to distinguish between the cases $H_2 > 0$ and $H_2 = 0$ for evaluating the function $\mathcal{P}$ that appears in (88). In the case $H_2 > 0$, we have $\mathcal{B}_2 = \mathrm{dev}(\mathbb{R}^{3\times 3}_s)$ from (64). Hence the function $\mathcal{P}$ defined in (86) is given by

$$\left\{ \begin{array}{l} \mathcal{P}(0) = 0, \\ \mathcal{P}(\boldsymbol{E}) = \infty \text{ if } \boldsymbol{E} \neq 0. \end{array} \right. \tag{89}$$

As a consequence of (89), the right hand side of (88) is infinite for any history $\boldsymbol{d}$ such that $\boldsymbol{E}_2 = \int_0^T \boldsymbol{d}_2 dt \neq 0$. It follows that

$$m_K = \inf_{\boldsymbol{d}} \int_\Omega \int_0^T R \max(\|\boldsymbol{d}_1\|, \frac{\|\boldsymbol{d}_2\|}{\kappa}) dvdt \tag{90}$$

where the infimum is taken over histories $\boldsymbol{d} = (\boldsymbol{d}_1, \boldsymbol{d}_2) \in (\mathrm{dev}(\mathbb{R}^{3\times 3}_s))^2$ such that

$$\int_0^T \int_\Omega \boldsymbol{\sigma}^E : \boldsymbol{d}_1 dvdt = 1, \int_0^T \boldsymbol{d}_1 dt = 0 \tag{91}$$

and $\int_0^T \boldsymbol{d}_2 dt = 0$. Since $\max(\|\boldsymbol{d}_1\|, \|\boldsymbol{d}_2\|/\kappa) \geq \|\boldsymbol{d}_1\|$, the infimum in (92) is clearly attained for $\boldsymbol{d}_2 = 0$, i.e we have

$$m_K = \inf_{\boldsymbol{d}_1} \int_\Omega \int_0^T R\|\boldsymbol{d}_1\| dv dt \tag{92}$$

where the infimum is taken over histories $\boldsymbol{d}_1$ satisfying (91).

In the case $H_2 = 0$, we have $\mathcal{B}_2 = \{\boldsymbol{\tau} \in \mathrm{dev}(\mathbb{R}^{3\times 3}_s) : \|\boldsymbol{\tau}\| \leq \tau_M\}$ from (64). Consequently, $\mathcal{P}(\boldsymbol{E}_2) = \tau_M \|\boldsymbol{E}_2\|$ and

$$m_K = \inf_{\boldsymbol{d}} \int_\Omega \int_0^T R \max(\|\boldsymbol{d}_1\|, \frac{\|\boldsymbol{d}_2\|}{\kappa}) dv dt + \int_\Omega \tau_M \|\boldsymbol{E}_2\| dv$$

where the infimum is taken over histories $\boldsymbol{d}$ satisfying (91). Again the infimum is attained for $\boldsymbol{d}_2 = 0$ so that the expression (92) remains valid.

5.3.2. Model of Barrera et al. (2014)

From the expression (32) of the elasticity domain, it can be calculated that the function $\mathcal{D}$ in (82) is given by

$$\mathcal{D}(\boldsymbol{d}) = R\left(\|\boldsymbol{d}_2\| + \frac{\|\boldsymbol{d}_1 + \boldsymbol{d}_2\|}{\kappa}\right).$$

In the case $H > 0$, we have $\mathcal{B}_2 = \mathrm{dev}(\mathbb{R}^{3\times 3}_s)$ from (69), hence $\mathcal{P}$ is given as in (89). Recalling that $\mathbb{K}_1 = -a\mathbb{K}$, $\mathbb{K}_2 = -(1+a)\mathbb{K}$ for the model of Barrera et al. (2014), we obtain

$$m_K = \inf_{\boldsymbol{d}} \int_\Omega \int_0^T R\left(\|\boldsymbol{d}_2\| + \frac{\|\boldsymbol{d}_1 + \boldsymbol{d}_2\|}{\kappa}\right) dv dt \tag{93}$$

where the infimum is taken over histories $\boldsymbol{d}$ such that

$$-\int_0^T \int_\Omega \boldsymbol{\sigma}^E : (a\boldsymbol{d}_1 + (1+a)\boldsymbol{d}_2)\, dv dt = 1, \int_0^T \boldsymbol{d}_1 dt = \int_0^T \boldsymbol{d}_2 dt = 0. \tag{94}$$

In the case $H = 0$, we have $\mathcal{P} = 0$ from (69). It follows that m_K is given by the same expression as (93) except that the infimum is taken over histories $\boldsymbol{d}$ satisfying

$$-\int_0^T \int_\Omega \boldsymbol{\sigma}^E : (a\boldsymbol{d}_1 + (1+a)\boldsymbol{d}_2)\, dv dt = 1, \int_0^T \boldsymbol{d}_1 dt = 0, \int_0^T \boldsymbol{d}_2 dt \in \mathcal{K}^0_\epsilon. \tag{95}$$

It can be observed that the requirements set on $\boldsymbol{d}_2$ in (95) are less stringent than those in (94). The value of m_K corresponding to $H = 0$ is thus lower than the value corresponding to $H > 0$.

6. Study of a three-bar truss structure

We consider the three-bar truss structure represented in Fig. 3. The bars have the same cross-sectional area S and are free to rotate at both extremities (pinned connections). The length of the middle bar (labelled as bar 1) is $l_1 = l$. The lengths of the two other bars (labelled as bars 2 and 3) are $l_2 = l_3 = l/\cos\theta$ where $\theta \in [0, \pi/2]$ is the angle between bar 1 and bar 2.

The structure is submitted to a vertical time-varying force $P(t)$ that varies periodically between 0 and a loading parameter $P_{max} > 0$. To fix ideas we take

$$P(t) = \frac{P_{max}}{2}(1 + \sin 2\pi \frac{t}{T}).$$

The stress field in each bar is assumed to be uniform and uniaxial, i.e. the stress in bar i can be written as $\sigma_i(t)\boldsymbol{n}_i \otimes \boldsymbol{n}_i$ where $\boldsymbol{n}_i$ is a unit vector along the axis of bar i. Correspondingly, the deviatoric stress in bar i is equal to $\sigma_i(t)(\boldsymbol{n}_i \otimes \boldsymbol{n}_i - \mathbf{1}/3)$. In such condition, the equilibrium implies that

$$\sigma_1(t) + (\sigma_2(t) + \sigma_3(t))\cos\theta = p(t) \tag{96}$$

where $p(t) = P(t)/S$. Under the assumption of infinitesimal strains, the geometric compatibility of the deformations in the bars implies that

$$\varepsilon_2(t) = \varepsilon_3(t) = \varepsilon_1(t)\cos^2\theta. \tag{97}$$

where $\varepsilon(i)$ is the strain along the axis of bar i.

Assuming the elasticity tensor to be isotropic, the fictitious elastic response $\boldsymbol{\sigma}^E(t)$ of the structure is obtained by solving (96) and (97) with the additional requirement that $\sigma_i(t) = E\varepsilon_i(t)$ where E is the Young's modulus. It follows that

$$\sigma_1^E(t) = \frac{p(t)}{1 + 2\cos^3\theta}\ ,\ \sigma_2^E(t) = \sigma_3^E(t) = \frac{p(t)\cos^2\theta}{1 + 2\cos^3\theta}. \tag{98}$$

From (96), stress fields $\boldsymbol{\rho}$ in $\mathcal{K}_\sigma^0$ are characterized by the relation

$$\rho_1 + (\rho_2 + \rho_3)\cos\theta = 0 \tag{99}$$

Strain fields in $\mathcal{K}_\epsilon^0$ are characterized by (97).

6.1. Shakedown limits

Let us first calculate the shakedown limit for the model of Auricchio et al. (2007). In order to evaluate the static coefficient m_S in (67), the radius $\gamma(\boldsymbol{x})$ of the curve $t \mapsto \boldsymbol{s}^E(\boldsymbol{x}, t)$ needs to be calculated in each bar. In bar 1, the deviatoric stress $\boldsymbol{s}^E$ describes the line segment $[0, p'_{max}](\boldsymbol{n}_1 \otimes \boldsymbol{n}_1 - \frac{1}{3}\mathbf{1})$ where

$$p'_{max} = \frac{p_{max}}{1 + 2\cos^3\theta}$$

and $p_{max} = P_{max}/S$. It follows that the radius γ_1 of the curve $t \mapsto \boldsymbol{s}^E(\boldsymbol{x}, t)$ in bar 1 is

$$\gamma_1 = \frac{1}{2} p'_{max} \|\boldsymbol{n}_1 \otimes \boldsymbol{n}_1 - \frac{1}{3}\mathbf{1}\| = \frac{1}{2} p'_{max} \sqrt{\frac{2}{3}}.$$

A similar calculation shows that the radius γ_2 (resp. γ_3) of the curve $t \mapsto \boldsymbol{s}^E(\boldsymbol{x}, t)$ in bar 2 (resp 3) is

$$\gamma_2 = \gamma_3 = \frac{1}{2} p'_{max} \cos^2\theta \sqrt{\frac{2}{3}}.$$

It follows from expression (65) that

$$m_S = \frac{R}{\max(\gamma_1, \gamma_2, \gamma_3)} = \frac{2k}{p'_{max}}$$

where $k = \sqrt{3/2}R$. Shakedown occurs if $m_S > 1$, i.e. if $p'_{max} < 2k$. The shakedown limit p_{SD} on the loading parameter p_{max} is thus equal to

$$p_{SD} = 2k(1 + 2\cos^3\theta). \tag{100}$$

Let us consider now the model of Barrera et al. (2014) as considered in Sect. 2.2. In the case $H > 0$, an analysis similar to that presented for the model of Auricchio et al. (2007) leads to

$$p_{SD} = \frac{2k}{\max(1, a\kappa)}(1 + 2\cos^3\theta).$$

In the case $H = 0$, the static coefficient m_S is given (75) and can not be evaluated in a simple fashion. However, a lower bound m_S^- can be obtained relatively simply by choosing $\boldsymbol{\rho}_* = 0$ in (75), i.e.

$$m_S^- = \sup_{(m, \boldsymbol{B}_1(\boldsymbol{x})) \in \mathbb{R} \times \operatorname{dev} \mathbb{R}_s^{3\times 3}} m \tag{101}$$

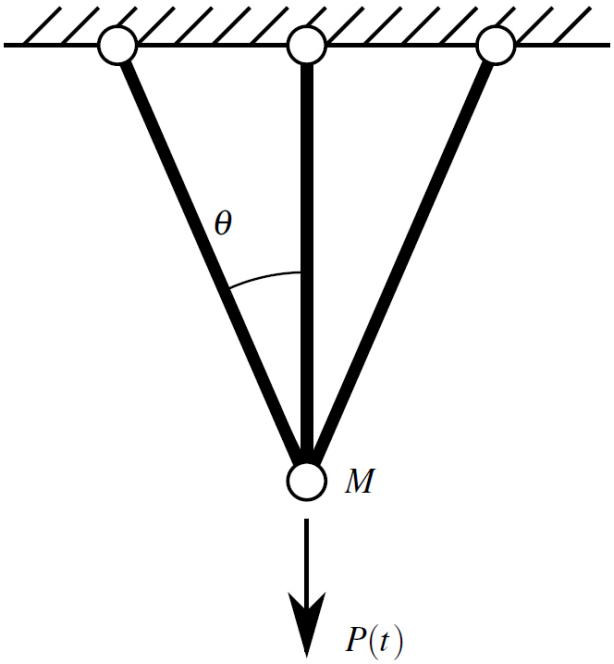

Figure 3: Three-bar truss.

where the supremum is taken over $(m, \boldsymbol{B}_1(\boldsymbol{x}))$ verifying

$$\sup_t \max\left\{\|m\boldsymbol{s}^E(\boldsymbol{x},t) - \boldsymbol{B}_1\|, \kappa\|ma\boldsymbol{s}^E(\boldsymbol{x},t) - \boldsymbol{B}_1\|\right\} \leq R \tag{102}$$

for all $\boldsymbol{x}$ and t. Consider a material point $\boldsymbol{x}$ in bar 1 and take $\boldsymbol{B}_1(\boldsymbol{x})$ in the form $B_1(\boldsymbol{n}_1 \otimes \boldsymbol{n}_1 - \frac{1}{3}\mathbf{1})$. Condition (102) gives

$$|m\frac{p(t)}{1+2\cos^3\theta} - B_1| \leq k \text{ and } \kappa|ma\frac{p(t)}{1+2\cos^3\theta} - B_1| \leq k \tag{103}$$

for all time t. Eq. (103) can be rewritten as

$$\begin{aligned} -k + m\frac{p(t)}{1+2\cos^3\theta} \leq B_1 \leq k + m\frac{p(t)}{1+2\cos^3\theta} \\ -\frac{k}{\kappa} + ma\frac{p(t)}{1+2\cos^3\theta} \leq B_1 \leq \frac{k}{\kappa} + ma\frac{p(t)}{1+2\cos^3\theta} \end{aligned} \qquad \forall t \tag{104}$$

Since $p(t)$ varies between 0 and p_{max}, Eq. (104) is equivalent to

$$-k + mp'_{max} \leq B_1 \leq k \text{ and } -\frac{k}{\kappa} + map'_{max} \leq B_1 \leq \frac{k}{\kappa}. \tag{105}$$

Some values B_1 satisfying (105) can be found if and only if

$$\max(-k + mp'_{max}, -\frac{k}{\kappa} + map'_{max}) \leq \min(k, \frac{k}{\kappa}). \tag{106}$$

For simplicity we only consider the case $0 < a \leq 1$, $0 < \kappa \leq 1$. Eq (106) becomes

$$-k + mp'_{max} \leq k \tag{107}$$

i.e. $mp'_{max} \leq 2k$. A similar analysis shows that condition (102) is satisfied in bars 2 and 3 if and only if $mp'_{max} \cos^2\theta \leq 2k$. It follows that the lower bound m_S^- in (101) is

$$m_S^- = \frac{2k}{p'_{max}}. \tag{108}$$

In contrast with the case $H > 0$, only a lower bound on m_S is available at this point. The exact value of m_S can be obtained by combining (108) with the kinematic approach presented in Sect. 5. Consider indeed the history $\boldsymbol{d}(\boldsymbol{x}, t) = (\boldsymbol{d}_1(\boldsymbol{x}, t), \boldsymbol{d}_2(\boldsymbol{x}, t))$ defined by $\boldsymbol{d}_2 = -\boldsymbol{d}_1$ and

$$\boldsymbol{d}_1(\boldsymbol{x}, t) = \eta_i \left(\delta(t) - \delta(t - T)\right) \left(\boldsymbol{n}_i \otimes \boldsymbol{n}_i - \frac{1}{3}\mathbb{1}\right) \tag{109}$$

for $\boldsymbol{x}$ in bar i. In (109), δ denotes the Dirac distribution and η_i is a constant ($i = 1, 2, 3$). Note that we have $\int_0^T \boldsymbol{d}_1(\boldsymbol{x}, t)dt = \int_0^T \boldsymbol{d}_2(\boldsymbol{x}, t)dt = 0$ at each point $\boldsymbol{x}$. The constants η_i in (109) are chosen in such a way that $-\int_0^T \int_\Omega \boldsymbol{\sigma}^E : (a\boldsymbol{d}_1 + (1 + a)\boldsymbol{d}_2)dvdt = 1$, i.e.

$$1 = \frac{2}{3} p'_{max} lS(\eta_1 + (\eta_2 + \eta_3)\cos\theta). \tag{110}$$

By Eqs (93) and (95), any (η_1, η_2, η_3) satisfying (110) provides an upper bound m_K^+ on m_K as

$$m_K^+ = \int_0^T \int_\Omega R\|\boldsymbol{d}_2(\boldsymbol{x}, t)\| d\boldsymbol{x}dt = R\sqrt{\frac{2}{3}} 2lS \left(|\eta_1| + \frac{1}{\cos\theta}(|\eta_2| + |\eta_3|)\right). \tag{111}$$

The best bound is obtained by minimizing (111) over (η_1, η_2, η_3) satisfying (110). It can be verified that the optimal values are $\eta_1 = 3/(2p'_{max} lS)$, $\eta_2 = \eta_3 = 0$, giving

$$m_K^+ = \frac{2k}{p'_{max}}. \tag{112}$$

Since $m_S^- \leq m_S \leq m_K \leq m_K^+$ and observing from (108) and (112) that $m_S^- = m_K^+$, we can conclude that

$$m_S = m_K = \frac{2k}{p'_{max}}.$$

The shakedown limit on the loading parameter p_{max} is thus given by (100).

Remark: For the model of Auricchio et al. (2007), the value of m_S obtained previously can also be recovered from the kinematic approach by considering a history $\boldsymbol{d}(\boldsymbol{x},t) = (-\boldsymbol{d}_1(\boldsymbol{x},t), 0)$ where $\boldsymbol{d}_1$ is taken in the form (109)-(110). This choice leads to the equality $m_S = m_K = 2k/p'_{max}$.

6.2. Step-by-step analysis

In this Section are presented some numerical results of the step-by-step analysis of the 3-bar truss. This requires to specify the initial state in each bar, which is chosen as $\boldsymbol{\alpha}_1 = \boldsymbol{\alpha}_2 = 0$ unless stated otherwise. The model of Auricchio et al. (2007) with material parameters in Table 1 is used. The presented results have been obtained using the algorithm of Peigney et al. (2018) for solving the incremental problem at each time step. The angle θ is set to $\pi/6$, in which case the shakedown limit p_{SD} in (100) is approximatively equal to 282 MPa.

Table 1: Material parameters

E (MPa)	ν -	τ_M (MPa)	H_1 (MPa)	H_2 (MPa)	A (MPa)	ϵ_L -	R (MPa)	κ -
50000	0.28	30	1000	15000	2000	0.04	50	10

Let us first consider the case $p_{max} = 250$ MPa, i.e. below the shakedown limit. For that value of the loading parameter, numerical simulations show that the evolution in bars 2 and 3 remains elastic. In Fig. 4(left) is plotted the calculated evolution of the internal variables $\boldsymbol{\alpha}_1$ and $\boldsymbol{\alpha}_2$ in bar 1. The tensor $\boldsymbol{\alpha}_i$ is parallel to $\boldsymbol{n} \otimes \boldsymbol{n} - \mathbf{1}/3$ in each bar, so that only the component of $\boldsymbol{\alpha}_i$ along $\boldsymbol{n} \otimes \boldsymbol{n} - \mathbf{1}/3$ is represented in Fig. 4(left). As expected, the internal variables converge towards a time-independent limit. Accordingly, the total dissipated energy remains bounded, see Fig. 4(right).

In Fig. 5(left) is plotted the evolution of the internal variables in the case $p_{max} =$ 600 MPa, i.e. above the shakedown limit. The evolution of the total dissipated energy is shown in Fig. 5(right). As expected, the total dissipated energy grows unbounded. The numerical results in Fig. 5(left) suggest that the internal variables converge towards a cyclic steady-state as t tends to infinity. This can be seen more clearly in Fig. 6 in which only the last 50 calculated cycles are shown. In each bar, the internal variable $\boldsymbol{\alpha}_2$ seems to converge towards a time-independent limit whereas $\boldsymbol{\alpha}_1$ becomes periodic.

We emphasize that shakedown occurs *independently of the initial state* for any loading parameter p_{max} below the shakedown limit provided by the theorems. To

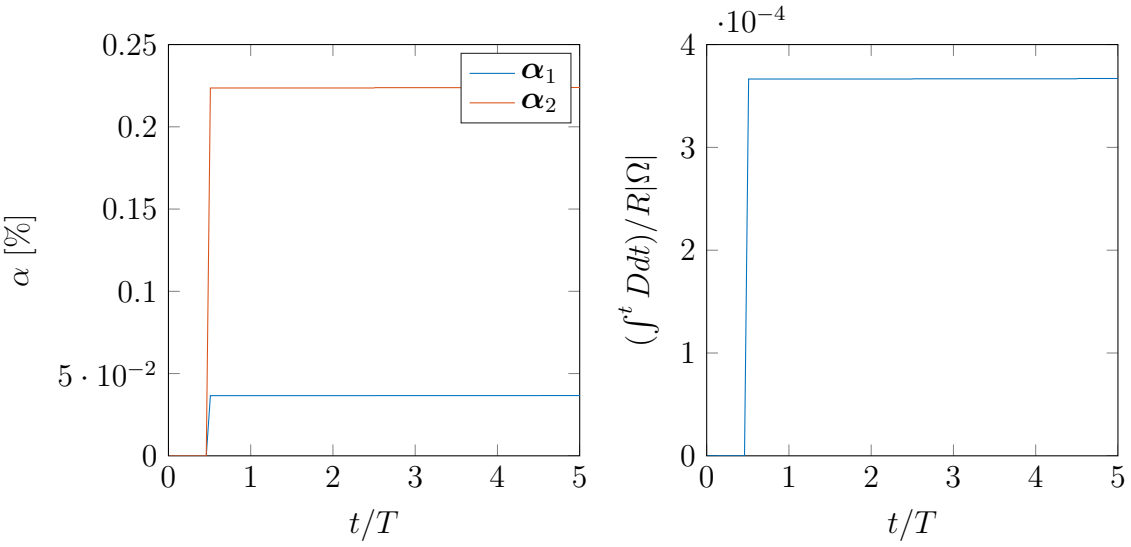

Figure 4: Evolution of the internal variables in bar 1(left). Evolution of the total dissipated energy (right). Case $p_{max} = 250$ MPa.

illustrate that point, the evolution of the internal variables is shown in Fig. 7 for $p_{max} = 250$ MPa with the initial state $\alpha_1 = -0.02$, $\alpha_2 = -0.01$ in bar 1 and $\alpha_1 = -0.015$, $\alpha_2 = -0.075$ in bars 2 and 3. The evolution of the internal variables in bar 1 (resp. bars 2 and 3) is shown in Fig. 7(left) (resp. Fig. 7(right)). We can observe that shakedown occurs (as in Fig. 4) even though details of the incremental evolution differ from Fig. 4. In other words, the initial state has an influence of the asymptotic values reached by the internal variables in the shakedown state.

7. Application to self-expanding nitinol stents

7.1. Cyclic pressure

We consider a stent geometry inspired by commercial nitinol stents and designed by Bonsignore (2021). The stent model, shown in Fig. 8, has an outer diameter D^0 of 8 mm, an inner diameter of 7.889 mm and a length L of 13.64 mm. It is composed of series of "strut Vs", arranged periodically and wrapped around a cylinder. There are 21 "strut Vs" around the circumference and 10 in the axial direction. Two adjacent rings of "strut Vs" are connected by 7 bridges around the circumference.

The nominal diameter D^0 of the stent is chosen larger to the vessel inner diameter D^1, so that once implanted the stent is constrained by the arterial wall and applies some outward forces on it (Duerig et al., 2000). Over a cardiac cycle, the

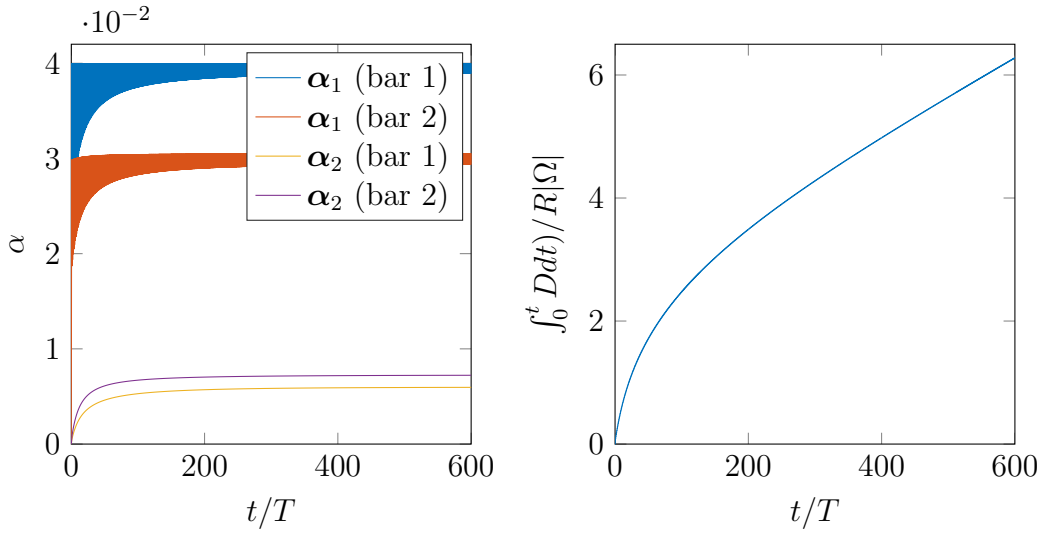

Figure 5: Evolution of the internal variables (left). Evolution of the total dissipated energy (right). Case $p_{max} = 600$ MPa.

arterial blood pressure varies between a minimum (diastolic) value p_d and a maximum (systolic) value p_s. As a result, the balanced diameter of the stent/artery varies between a minimum (diastolic) value D_d and a maximum (systolic) value D_s such that $D^1 < D_d < D_s < D^0$. Clinically relevant values of the diameter change $\Delta D = D_s - D_d$ are about 0.3 mm (Pelton et al., 2008).

To fix ideas, we use the model of Auricchio et al. (2007) in the following but the analysis can easily be transposed to the model of Barrera et al. (2014) as considered in Sect. 2.2. We evaluate the shakedown limit of the stent by calculating m_S in Eq. (67). The mechanical loading of the stent due to the combined action of the arterial wall and cardiac cycle is here modeled by a time-dependent net pressure $p(t)$ applied on the outer surface of the stent, as represented in Fig. 9(left). The corresponding fictitious elastic response $\boldsymbol{\sigma}^E$ is linear in p and can be written as

$$\boldsymbol{\sigma}^E(\boldsymbol{x}, t) = p(t)\tilde{\boldsymbol{\sigma}}_0^E(\boldsymbol{x}) \tag{113}$$

where

$$\tilde{\boldsymbol{\sigma}}_0^E = \frac{\boldsymbol{\sigma}_0^E}{p_0}$$

and $\boldsymbol{\sigma}_0^E$ is the elastic stress field corresponding to a (arbitrarily chosen) reference value p_0 of the applied pressure (note that $\tilde{\boldsymbol{\sigma}}_0^E$ is independent of p_0). Eq. (113) shows that $t \mapsto \boldsymbol{\sigma}^E(\boldsymbol{x}, t)$ lives on the vectorial line $\mathbb{R}\tilde{\boldsymbol{\sigma}}_0^E(\boldsymbol{x})$. The radius $\gamma(\boldsymbol{x})$ of the

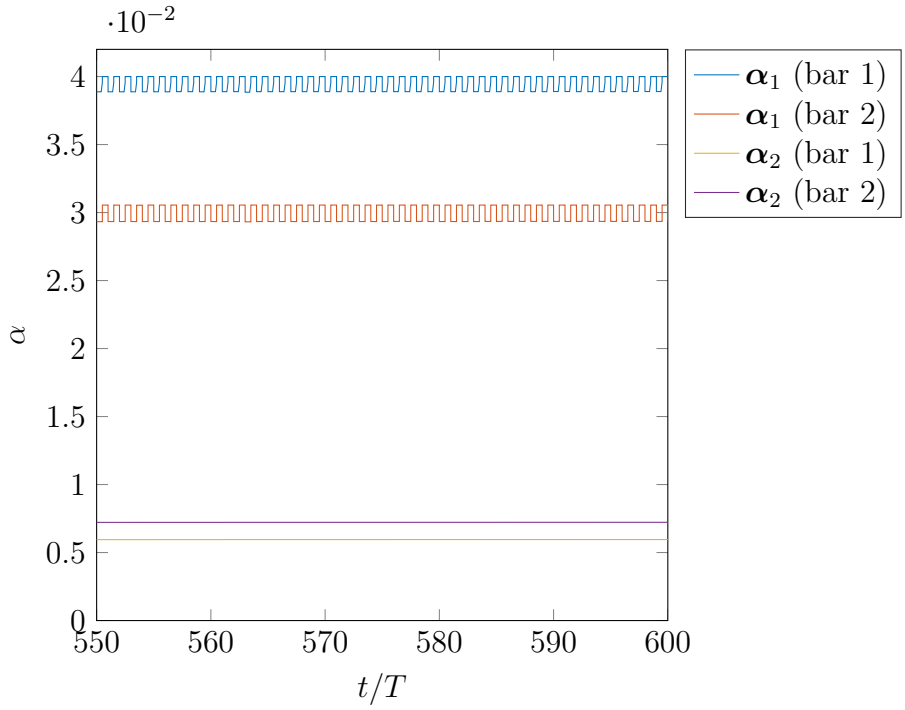

Figure 6: Evolution of the internal variables over loading cycles 550-600. Case $p_{max} = 600$ MPa.

curve $t \mapsto \boldsymbol{s}^E(\boldsymbol{x}, t)$ is thus equal to

$$\gamma(\boldsymbol{x}) = \frac{1}{2}(\max_t p - \min_t p)\|\tilde{\boldsymbol{s}}_0^E(\boldsymbol{x})\|$$

where $\tilde{\boldsymbol{s}}_0^E$ is the deviatoric part of $\tilde{\boldsymbol{\sigma}}_0^E$. Eq. (67) yields

$$m_S = \frac{2R}{\Delta p \sup_{\boldsymbol{x}} \|\tilde{\boldsymbol{s}}_0^E(\boldsymbol{x})\|} \tag{114}$$

with $\Delta p = \max_t p - \min_t p$. Shakedown is thus determined by the amplitude of the pressure $p(t)$, without any influence of the mean value. The shakedown limit Δp_{SD} on the loading amplitude Δp is equal to $2R/\sup_{\boldsymbol{x}} \|\tilde{\boldsymbol{s}}_0^E(\boldsymbol{x})\|$ and can be rewritten in terms of the Von Mises equivalent stress $\tilde{\sigma}_0^{eq}(\boldsymbol{x}) = \sqrt{3/2}\|\tilde{\boldsymbol{s}}_0^E(\boldsymbol{x})\|$ as

$$\Delta p_{SD} = \frac{\sqrt{6}R}{\sup_{\boldsymbol{x}} \tilde{\sigma}_0^{eq}(\boldsymbol{x})}. \tag{115}$$

Evaluating Δp_{SD} requires solving the linear elasticity problem defining $\boldsymbol{\sigma}_0^E$, which can performed using Finite Element Analysis (FEA). In Fig. 10 is shown the distribution

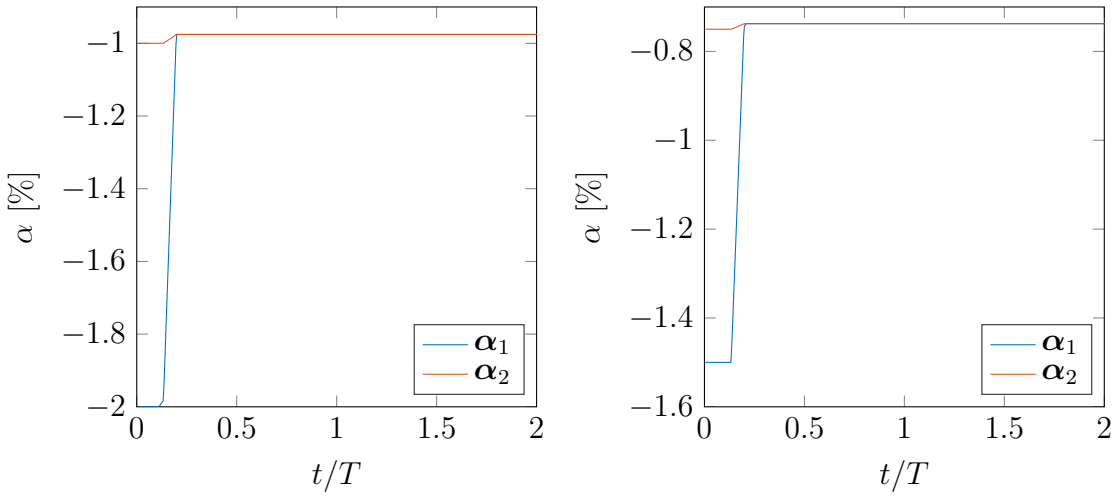

Figure 7: Evolution of the internal variables in bar 1(left) and bar 2 (right) starting from a non zero initial state. Case $p_{max} = 250$ MPa.

of the Von Mises equivalent stress as obtained from FEA with $p_0 = 100$ mmHg (13300 Pa). The maximum value of the Von Mises equivalent stress is 73.03 MPa. The value $E = 34000$ MPa and $\nu = 0.33$ have been used (Bonsignore, 2011). The FEA calculations have been performed in the software Solidworks using a tetrahedral mesh with 427631 elements (734832 nodes). For the reference pressure $p_0 = 100$ mmHg, FEA gives a diameter change ΔD_0 between the initial and deformed configuration of 0.1197 mm. The maximum value of the largest principal strain is 0.212 %. Adopting the value $R = 148$ MPa (Auricchio et al., 2016), Eq. (115) gives $\Delta p_{SD} = 496.4$ mmHg. The diameter change ΔD at the shakedown limit is $\Delta D_0(\Delta p_{SD}/p_0) \simeq 0.5942$ mm. This is about twice the value observed *in vivo* (0.3 mm). In terms of principal strain, the shakedown limit is 1.05% peak-to-peak amplitude, i.e. a variation of $\pm 0.52\%$ around the mean value. It is interesting to compare those predictions with the experimental results of Pelton et al. (2008) on the fatigue limit of stents. The authors performed cyclic pressure tests of various amplitudes and mean values. They obtained a 10^7 cycle fatigue strain amplitude limit of $\pm 0.4\%$. The effect of the mean strain on the fatigue limit only appears for relatively large values (mean strain above 1.5%). The observed independence of the fatigue limit with respect to the mean value is consistent with the results obtained from shakedown theory. The 10^7 cycle fatigue strain amplitude (0.4%) limit is smaller than the shakedown amplitude limit (0.52%), which is also consistent because shakedown can regarded as a necessary – but not sufficient – condition for unlimited (or very high) fatigue lifetime.

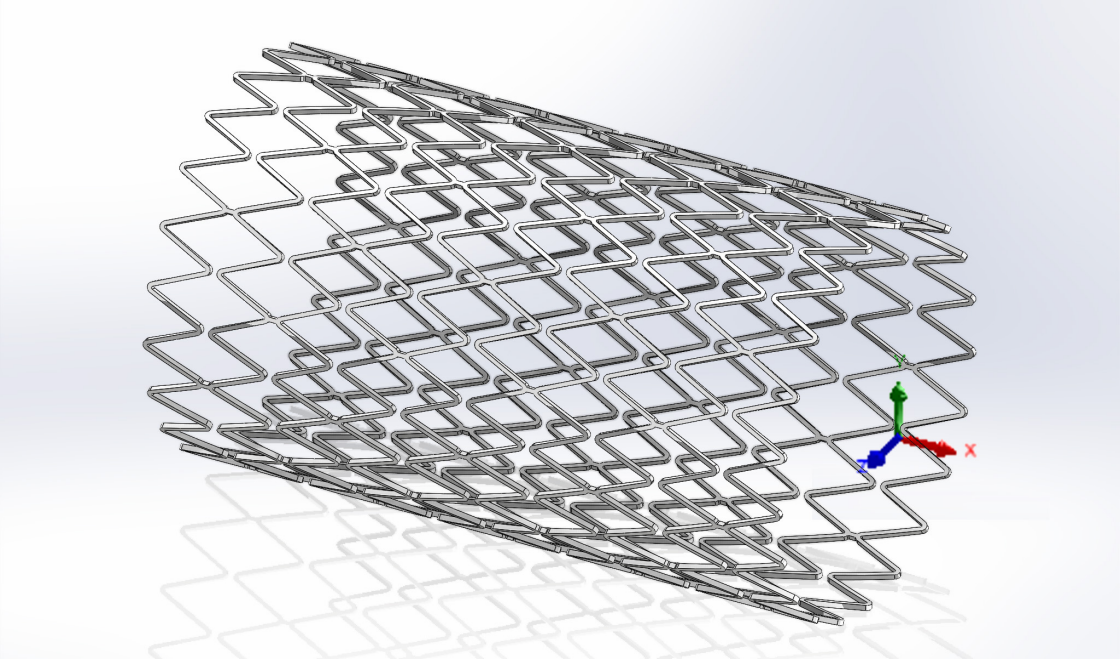

Figure 8: Geometry of the stent.

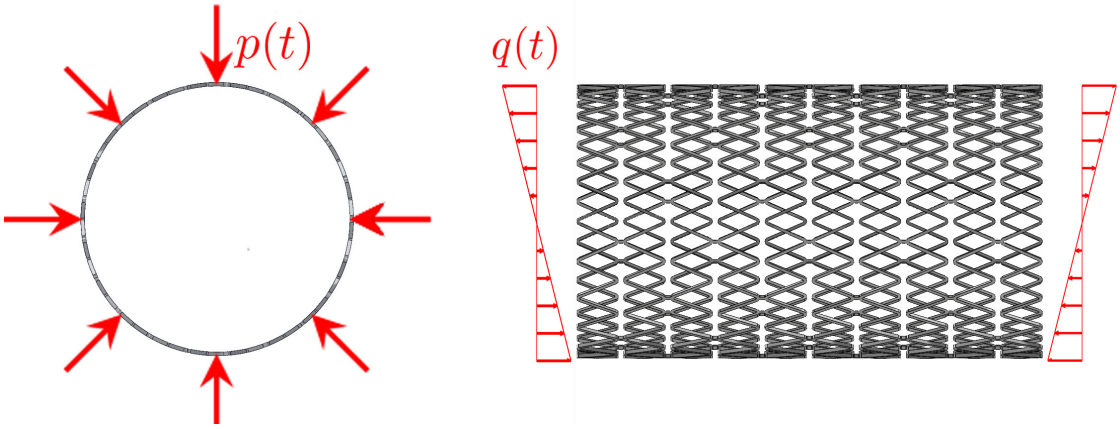

Figure 9: Boundary conditions applied on the stent.

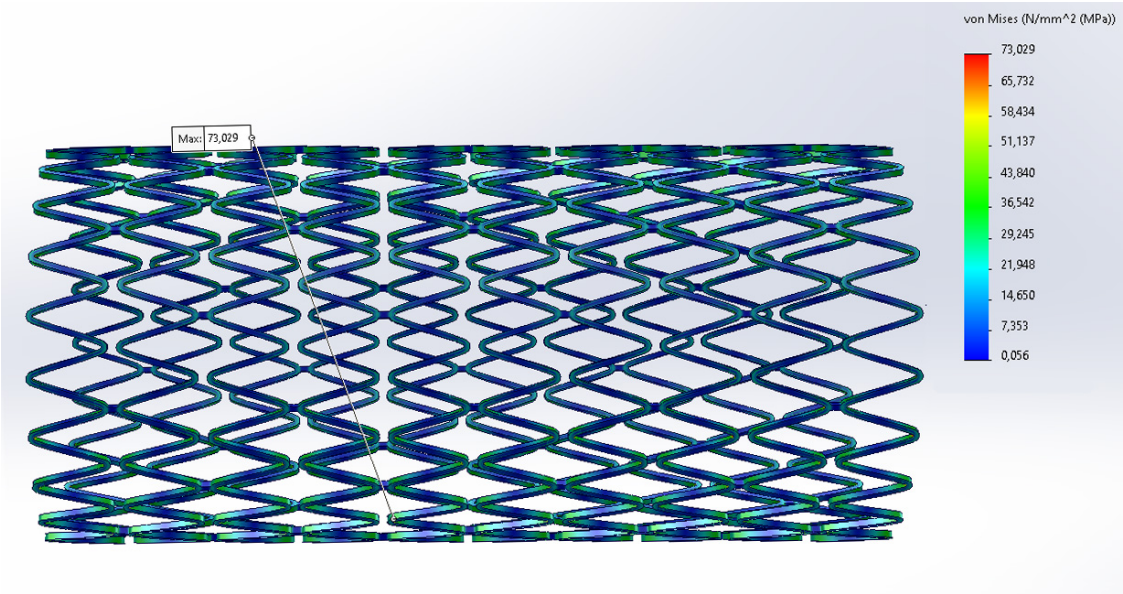

Figure 10: Von Mises equivalent stress distribution for an applied pressure $p_0 = 100$ mmHg.

7.2. Mixed pressure–bending

Regarding the expected *in vivo* lifetime of stents, the results obtained in Sect .7.1 from shakedown calculations are similar to the conclusions of Pelton et al. (2008): *in vivo* stents are submitted to loading amplitudes that are significantly smaller (by a factor in a range 1.7–2) than the critical limit. As advanced by Pelton et al. (2008), that conclusion should be mitigated by the fact that *in vivo* stents are submitted to loadings that are more complex than pure cyclic pressure. In addition to the pulsatile pressure due to the cardiac cycle, stents are also submitted to torsion/bending due to the motion of the human body. That multiaxial loading occurs at a relatively high frequency ($\sim$ 1 million cycles per year (Silva et al., 2002)) and therefore should be taken into account in fatigue analysis. An obstacle in doing so lies in the complexity of that additional multiaxial loading, notably the difficulty in obtaining details of its time-history. Bounds on the extreme values can reasonably be expected, however. Interestingly, the results of Sects 4 and 5 still remain useful in such situation where limited information on the loading is available. To illustrate that point, consider a mixed pressure–bending loading obtained by applying a pressure $p(t)$ on the outer diameter of the stent and tractions

$$q(t)\frac{2y}{D}\boldsymbol{e}_x \tag{116}$$

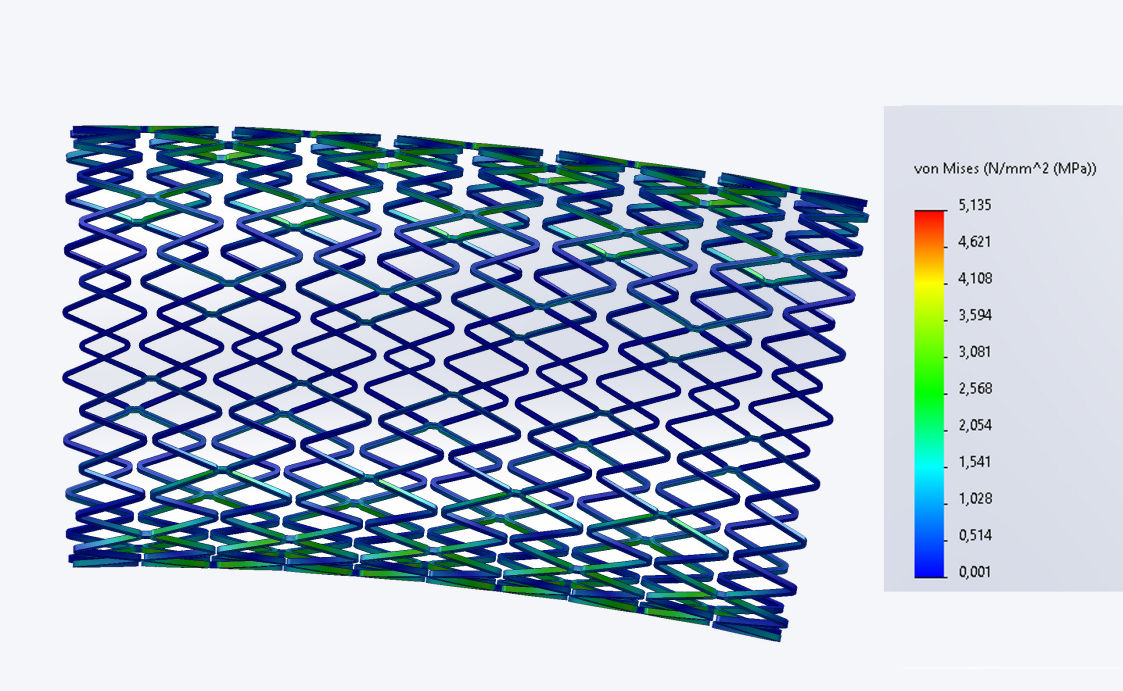

Figure 11: Von Mises equivalent stress distribution (plotted on the deformed configuration) in pure bending with $q_0 = 100$ mmHg. For a better visualization, an amplification factor of 28.8 is set to the deformation.

on the end section $x = 0$ (the coordinates axes are shown in Fig. 8). Tractions opposite to (116) are applied on the end section $x = -L$ to ensure equilibrium. The boundary conditions considered are represented in Fig. 9. Tractions (116) have zero resultant force and produce a bending moment around $\boldsymbol{e}_z$. The resulting bending angle is proportional to the loading parameter $q(t)$. We assume that $p(t)$ and $q(t)$ vary between known extreme values (p_-, p_+) and (q_-, q_+), i.e.

$$p_- \leq p(t) \leq p_+, \quad q_- \leq q(t) \leq q_+, \tag{117}$$

without specifying any more detail on the time-dependence of p and q.

Let $\boldsymbol{\sigma}_1^E$ be the fictitious elastic response for $(p(t), q(t)) = (0, q_0)$ where q_0 is an arbitrary chosen reference value. For that pure bending loading, the distribution of the Von Mises equivalent stress and the deformed geometry obtained from FEA are shown in Fig. 11. The value $q_0 = 100$ mmHg has been used. For that value of q_0, the obtained bending angle $\Delta\alpha_0$ is 0.39°. By the principle of superposition, the fictitious

elastic response $\boldsymbol{\sigma}^E$ corresponding to an arbitrary time-history $(p(t), q(t))$ is

$$\boldsymbol{\sigma}^E(\boldsymbol{x}, t) = p(t)\tilde{\boldsymbol{\sigma}}_0^E(\boldsymbol{x}) + q(t)\tilde{\boldsymbol{\sigma}}_1^E(\boldsymbol{x})$$

where $\tilde{\boldsymbol{\sigma}}_1^E = \boldsymbol{\sigma}_1^E/q_0$. Let $\tilde{\boldsymbol{s}}_1^E$ be the deviatoric part of $\tilde{\boldsymbol{\sigma}}_1^E$. In view of (117), the curve $t \mapsto \boldsymbol{s}^E(\boldsymbol{x}, t)$ at any given location $\boldsymbol{x}$ is inscribed in the parallelogram with corners $p_\pm\tilde{\boldsymbol{s}}_0^E(\boldsymbol{x}) + q_\pm\tilde{\boldsymbol{s}}_1^E(\boldsymbol{x})$ as represented in Fig 12. The radius $\gamma(\boldsymbol{x})$ of the curve

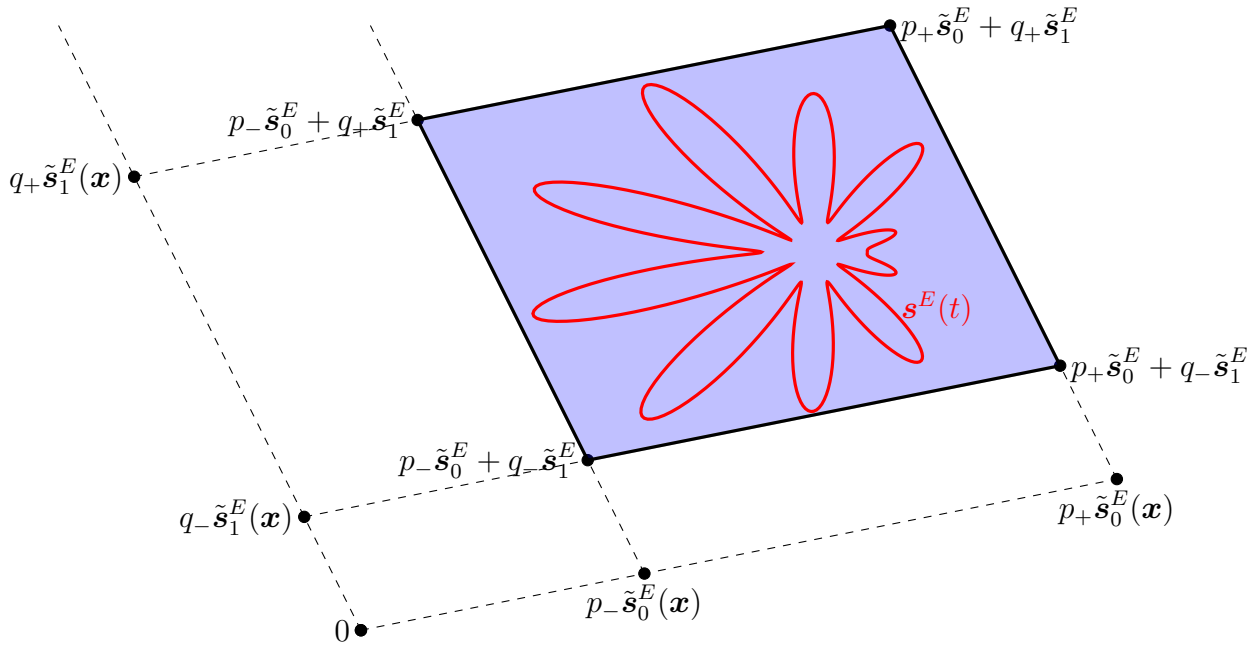

Figure 12: Pointwise bound on the radius $\gamma(t)$ of the curve $t \mapsto \boldsymbol{s}^E(\boldsymbol{x}, t)$ in the case of 2 loadings parameters.

$t \mapsto \boldsymbol{s}^E(\boldsymbol{x}, t)$ is thus smaller than the radius of the mentioned parallelogram, i.e. verifies

$$\gamma(\boldsymbol{x}) \leq \frac{1}{2}\max\left(\|\Delta p\,\tilde{\boldsymbol{s}}_0^E(\boldsymbol{x}) + \Delta q\,\tilde{\boldsymbol{s}}_1^E(\boldsymbol{x})\|, \|\Delta p\,\tilde{\boldsymbol{s}}_0^E(\boldsymbol{x}) - \Delta q\,\tilde{\boldsymbol{s}}_1^E(\boldsymbol{x})\|\right) \tag{118}$$

where $\Delta p = p_+ - p_-$ and $\Delta q = q_+ - q_-$. Eq. (67) yields

$$m_S = \frac{2R}{\sup_{\boldsymbol{x}} \max\left(\|\Delta p\,\tilde{\boldsymbol{s}}_0^E(\boldsymbol{x}) + \Delta q\,\tilde{\boldsymbol{s}}_1^E(\boldsymbol{x})\|, \|\Delta p\,\tilde{\boldsymbol{s}}_0^E(\boldsymbol{x}) - \Delta q\,\tilde{\boldsymbol{s}}_1^E(\boldsymbol{x})\|\right)}$$

The shakedown condition $m_S > 1$ can thus be written as

$$(\Delta p)^2 \|\tilde{\boldsymbol{s}}_0^E(\boldsymbol{x})\|^2 + (\Delta q)^2 \|\tilde{\boldsymbol{s}}_1^E(\boldsymbol{x})\|^2 + 2\Delta p \Delta q |\tilde{\boldsymbol{s}}_0^E(\boldsymbol{x}) : \tilde{\boldsymbol{s}}_1^E(\boldsymbol{x})| < 4R^2 \tag{119}$$

for all $\boldsymbol{x}$. For a given $\boldsymbol{x}$, Eq. (119) defines an ellipse in the plane $(\Delta p, \Delta q)$. The shakedown domain in the plane $(\Delta p, \Delta q)$ is thus obtained by taking the intersection of the ellipses defined by (119) for all $\boldsymbol{x}$. A convenient way to calculate that multiple sets intersection is to use a polar representation, writing $(\Delta p, \Delta q)$ in the form $(\Delta p, \Delta q) = (r\cos\theta, r\sin\theta)$ with $r \geq 0$ and $\theta \in [0, \pi/2]$. From (119) we obtain that shakedown occurs if

$$\frac{r^2}{4R^2} < \left(\cos^2\theta \|\tilde{\boldsymbol{s}}_0^E(\boldsymbol{x})\|^2 + \sin^2\theta \|\tilde{\boldsymbol{s}}_1^E(\boldsymbol{x})\|^2 + 2\cos\theta\sin\theta |\tilde{\boldsymbol{s}}_0^E(\boldsymbol{x}) : \tilde{\boldsymbol{s}}_1^E(\boldsymbol{x})|\right)^{-1}$$

for all $\boldsymbol{x}$, i.e. if

$$\frac{r^2}{4R^2} < \inf_{\boldsymbol{x}} \left(\cos^2\theta \|\tilde{\boldsymbol{s}}_0^E(\boldsymbol{x})\|^2 + \sin^2\theta \|\tilde{\boldsymbol{s}}_1^E(\boldsymbol{x})\|^2 + 2\cos\theta\sin\theta |\tilde{\boldsymbol{s}}_0^E(\boldsymbol{x}) : \tilde{\boldsymbol{s}}_1^E(\boldsymbol{x})|\right)^{-1}. \tag{120}$$

Eq. (120) is the polar representation of the shakedown domain in the plane $(\Delta p, \Delta q)$. The right hand side of (120) can easily be evaluated from FEA and requires only 2 elastic calculations (for obtaining the stress fields $\tilde{\boldsymbol{\sigma}}_0^E$ and $\tilde{\boldsymbol{\sigma}}_1^E$). The shakedown domain obtained in such fashion is shown in Fig. 13. To ease the interpretation, the results in Fig. 13 are reported in terms of the diameter change $\Delta D = \Delta D_0(\Delta p/p_0)$ and the bending angle change $\Delta\alpha = \Delta\alpha_0(\Delta q/q_0)$. For $\Delta D = 0$ (pure bending), the shakedown limit on the bending angle change $\Delta\alpha$ is approximatively 27.5°. For $\Delta\alpha$ (pure pressure), the shakedown limit obtained in Sect. 7.1 on the diameter change ΔD is recovered, i.e. $\Delta D \simeq 0.5942$ mm. The results in Fig. 13 show that combined bending–pressure is more severe than bending or pressure alone. To illustrate that point, consider the clinically relevant value $\Delta\alpha = 0.3$ mm. For that value of ΔD, the shakedown limit on the bending angle change $\Delta\alpha$ is approximatively 15°. If the *in vivo* bending angle change is significantly above that limit value, then a significant reduction of the fatigue life of the stent is to be expected compared to the $> 10^7$ cycles limit corresponding to pure pressure.

8. Concluding remarks

In this paper, we have presented static and kinematic shakedown theorems for SMA models coupling phase-transformation with permanent inelasticity and degradation effects. We emphasize that those theorems are path-independent: the obtained shakedown conditions apply whatever the initial state of the system (which

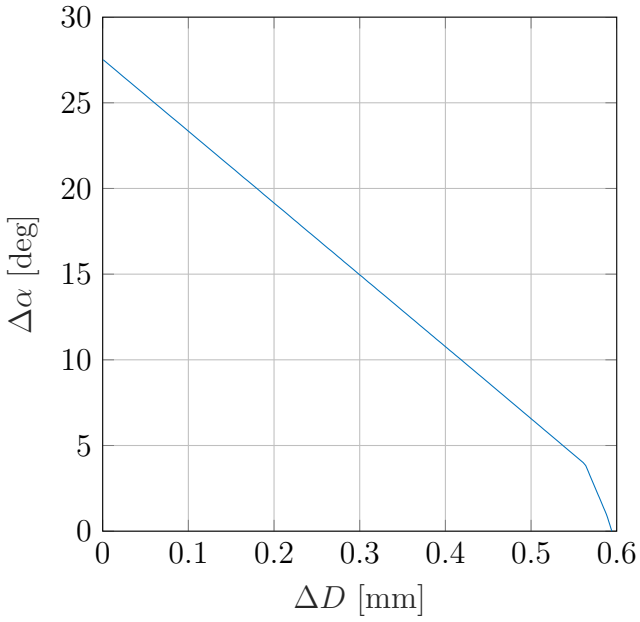

Figure 13: Shakedown limits in the plane $(\Delta p, \Delta\alpha)$.

for instance would correspond to some initial residual stress). Interestingly, the values of all the constitutive parameters entering the expression of the free energy are not needed for applying the shakedown theorems. For instance, the shakedown conditions for the model of Auricchio et al. (2007) do not depend on the constitutive parameters τ_M, H_1, H_2 and A of the free energy (15). For the model of Barrera et al. (2014) as considered in Sect. 2.2, the obtained shakedown conditions do not depend on τ_M and H in (22). The theorems presented are not restricted to those two material models and apply to any constitutive model that can be put in the format (10). This is notably the case of some micromechanical SMA models that have been proposed in the literature (Hackl and Heinen, 2008; Peigney, 2009, 2023). Those models capture effects such as anisotropy and tension-compression asymmetry which are often observed in SMAs. Tension-compression asymmetry can also modeled phenomelogically by considering a convex elasticity domain depending on the second- and third-invariant of the deviatoric stress, as proposed notably by Auricchio and Petrini (2004b); Raniecki and Mroz (2008). The format (10) allows for such dependence, hence no extension of the theoretical framework is needed for applying the shakedown theorems in such cases.

Although the proofs of the theorems are more involved than their counterpart in perfect plasticity, the final form of the shakedown conditions are not significantly

more complicated. This is especially true for the static approach which – at least for the material models presented – reduces to calculating the radius of a curve in the space of deviatoric stresses. Some efficient numerical algorithms are available for computing the smallest ball enclosing a given set of points in any dimension (Welzl, 2005; Matoušek et al., 1992; Scalet, 2018) and could be used in the present context.

Regarding fatigue design of structures, the approach presented has the attractive features of relying only on elastic calculations and being relatively simple to implement. It still can be used when limited information on the loading is available, as illustrated in Sect. 7.2. A limitation of the shakedown approach is that it does not provide a quantified estimate of the number of cycles to failure. To access such information, the shakedown approach needs to be combined with fatigue criteria, which are generally phenomenological in nature and involve additional constitutive parameters that need to be fitted from experiments (see e.g. Auricchio et al. (2016); Mahtabi and Shamsaei (2016) for some examples).

Among the possible developments of the work presented, it would be interesting to study other constitutive models of phase transformation / degradation effects than those considered presented in this paper, and to investigate whether path-independent shakedown theorems could still be obtained when some of the assumptions made in Sect. 2 are relaxed. In that regard, it should be noted that some effort on the modelling of SMAs is still needed to better capture the influence of the loading amplitude on functional fatigue as observed in experiments. As illustrated in Sect. 7, the approach presented could tentatively be useful for studying fatigue of stents under complex multiaxial loadings and it would be interesting to pursue efforts in that direction. As a final remark, we note that thermomechanical coupling plays a significant role in some SMA systems (Shaw and Kyriakides, 1995; Auricchio et al., 2008). Thermomechanical coupling profoundly changes the mathematical structure of the evolution problem, making it more difficult to solve and requiring dedicated numerical strategies (Yang et al., 2006; Peigney, 2006; Peigney and Seguin, 2013). It would be interesting – but certainly challenging – to study the extension of shakedown theorems to coupled thermomechanical evolutions of SMA structures.

Acknowledgements

The author is grateful to Jules Coquard, Paul Gauvrit and Théo Manière (Ecole Polytechnique) for setting up early versions of the stent finite-element model and for helpful discussions on that matter.

Appendix A. Calculation of $\mathcal{B}_2$ for the model of Auricchio et al. (2007)

The expression of the set $\mathcal{B}_2 = \{\boldsymbol{B}_2 | (\boldsymbol{B}_1, \boldsymbol{B}_2) \in \partial f(\boldsymbol{\alpha}), \boldsymbol{\alpha} \in \mathcal{T}\}$ is central for applying the shakedown theorems that have been presented. The set $\mathcal{B}_2$ depends on the material model under consideration. For the model of Auricchio et al. (2007), we show in this Appendix that

$$\mathcal{B}_2 = \begin{cases} \mathrm{dev}(\mathbb{R}^{3\times 3}_s) & \text{if } H_2 > 0, \\ \{\boldsymbol{\tau} | \mathrm{tr}\, \boldsymbol{\tau} = 0, \|\boldsymbol{\tau}\| \leq \tau_M\} & \text{if } H_2 = 0. \end{cases}$$

If $H_2 > 0$ we claim that $\mathcal{B}_2 = \mathrm{dev}(\mathbb{R}^{3\times 3}_s)$, i.e. for any $\boldsymbol{U}$ there exists $(\boldsymbol{\alpha}_1, \boldsymbol{\alpha}_2, \boldsymbol{B}_1)$ such that $\|\boldsymbol{\alpha}_1\| \leq \epsilon_L$ and $(\boldsymbol{B}_1, \boldsymbol{U}) \in \partial f(\boldsymbol{\alpha}_1, \boldsymbol{\alpha}_2)$. First assume that $\|\boldsymbol{U}\| \leq \tau_M$. Noting from expression (19) that

$$\partial f(0,0) = \{\tau_M(\boldsymbol{\tau}, -\boldsymbol{\tau}) | \mathrm{tr}\, \boldsymbol{\tau} = 0, \|\boldsymbol{\tau}\| \leq 1\}, \tag{A.1}$$

we obtain that $(-\boldsymbol{U}, \boldsymbol{U}) \in \partial f(0,0)$ and therefore that $\boldsymbol{U} \in \mathcal{B}_2$. If $\|\boldsymbol{U}\| > \tau_M$, consider the value $\boldsymbol{\alpha}_2$ given by

$$\boldsymbol{\alpha}_2 = \left(\frac{\|\boldsymbol{U}\| - \tau_M}{H_2} \right) \frac{\boldsymbol{U}}{\|\boldsymbol{U}\|}.$$

From (19), we obtain

$$\partial f(0, \boldsymbol{\alpha}_2) = \left(\left[-\tau_M - \frac{A}{H_2} (\|\boldsymbol{U}\| - \tau_M) \right] \frac{\boldsymbol{U}}{\|\boldsymbol{U}\|}, \boldsymbol{U} \right)$$

hence $\boldsymbol{U} \in \mathcal{B}_2$. This completes the proof that $\mathcal{B}_2 = \mathrm{dev}(\mathbb{R}^{3\times 3}_s)$.

The situation is different when $H_2 = 0$. First note from condition (18) that $H_2 = 0$ also implies that $A = 0$. In that case we claim that

$$\mathcal{B}_2 = \{\boldsymbol{\tau} | \mathrm{tr}\, \boldsymbol{\tau} = 0, \|\boldsymbol{\tau}\| \leq \tau_M\}.$$

Let indeed $\boldsymbol{U} \in \mathcal{B}_2$, i.e there exists $\boldsymbol{B}_1$ and $(\boldsymbol{\alpha}_1, \boldsymbol{\alpha}_2)$ be such that $\|\boldsymbol{\alpha}_1\| \leq \epsilon_L$ and $(\boldsymbol{B}_1, \boldsymbol{U}) \in \partial f(\boldsymbol{\alpha}_1, \boldsymbol{\alpha}_2)$. Eq. (19) gives $\|\boldsymbol{B}_1\| = \|\boldsymbol{U}\| \leq \tau_M$. It follows that $\mathcal{B}_2 \subset \{\boldsymbol{\tau} | \mathrm{tr}\, \boldsymbol{\tau} = 0, \|\boldsymbol{\tau}\| \leq \tau_M\}$. The reverse inclusion follows from (A.1).

References

Antonucci, V., Auricchio, F., Lecce, L., Sacco, E., et al., 2021. Shape memory alloy engineering: for aerospace, structural, and biomedical applications. Butterworth-Heinemann.

Artioli, E., Bisegna, P., 2016. An incremental energy minimization state update algorithm for 3d phenomenological internal-variable sma constitutive models based on isotropic flow potentials. International Journal for Numerical Methods in Engineering 105 (3), 197–220.

Auricchio, F., Constantinescu, A., Menna, C., Scalet, G., 2016. A shakedown analysis of high cycle fatigue of shape memory alloys. International Journal of Fatigue 87, 112–123.

Auricchio, F., Fugazza, D., Desroches, R., 2008. Rate-dependent thermo-mechanical modelling of superelastic shape-memory alloys for seismic applications. Journal of Intelligent Material Systems and Structures 19 (1), 47–61.

Auricchio, F., Petrini, L., 2004a. A three-dimensional model describing stress-temperature induced solid phase transformations: solution algorithm and boundary value problems. Int.J.Num.Meth.Eng. 61, 807–836.

Auricchio, F., Petrini, L., 2004b. A three-dimensional model describing stress-temperature induced solid phase transformations: solution algorithm and boundary value problems. International journal for numerical methods in engineering 61 (6), 807–836.

Auricchio, F., Reali, A., Stefanelli, U., 2007. A three-dimensional model describing stress-induced solid phase transformation with permanent inelasticity. Int.J. Plasticity 23, 207–226.

Barrera, N., Biscari, P., Urbano, M., 2014. Macroscopic modeling of functional fatigue in shape memory alloys. Eur.J.Mech. A.Solids.

Bauschinger, J., 1886. Ueber die veranderung der elasticitatsgrenge und der festigkeit des eisens und stahls durch strecken und quetschn, durch erwarmen und abkuhlen und durch oftmal wiederholte beanspruchung. Mitteilungen aus dem Mechanisch-Technischen Laboratorium der K. Technischen Hochschule in Munchen 13.

Bhattacharya, K., Kohn, R. V., 1997. Elastic energy minimization and the recoverable strains of polycrystalline shape-memory materials. Archive for Rational Mechanics and Analysis 139, 99–180.

Bonsignore, C., 2011. Open stent design. NDC 47533, 20–47.

Bonsignore, C., 2021. open-stent. `https://github.com/cbonsig/open-stent`.

Borino, G., 2000. Consistent shakedown theorems for materials with temperature dependent yield functions. International journal of solids and structures 37 (22), 3121–3147.

Chemisky, Y., Hartl, D. J., Meraghni, F., 2018. Three-dimensional constitutive model for structural and functional fatigue of shape memory alloy actuators. International Journal of Fatigue 112, 263–278.

Cisse, C., Zaki, W., Zineb, T. B., 2016. A review of constitutive models and modeling techniques for shape memory alloys. International Journal of Plasticity 76, 244–284.

Dornelas, V. M., Oliveira, S. A., Savi, M. A., 2020. A macroscopic description of shape memory alloy functional fatigue. International Journal of Mechanical Sciences 170, 105345.

Duerig, T., Tolomeo, D., Wholey, M., 2000. An overview of superelastic stent design. Minimally invasive therapy & allied technologies 9 (3-4), 235–246.

Eggeler, G., Hornbogen, E., Yawny, A., Heckmann, A., Wagner, M., 2004. Structural and functional fatigue of niti shape memory alloys. Materials Science and Engineering: A 378 (1-2), 24–33.

Feng, X., Sun, Q., 2007. Shakedown analysis of shape memory alloy structures. Int J. Plasticity 23, 183–206.

Flett, T., 1980. Differential analysis; differentiation, differential equations and differential inequalities. Cambridge University Press.

Frémond, M., 2002. Non-smooth thermomechanics. Springer.

Govindjee, S., Miehe, C., 2001. A multi-variant martensitic phase transformation model: formulation and numerical implementation. Comput. Methods Appl. Mech. Engrg. 191, 215–238.

Hackl, K., Heinen, R., 2008. An upper bound to the free energy of $n-$variant polycrystalline shape memory alloys. J.Mech.Phys.Solids 56, 2832–2843.

Halphen, B., Nguyen, Q., 1975. Sur les matériaux standards généralisés. J.Mécanique 14, 1–37.

Hasbroucq, S., Oueslati, A., de Saxcé, G., 2010. Inelastic responses of a two-bar system with temperature-dependent elastic modulus under cyclic thermomechanical loadings. International Journal of Solids and Structures 47 (14-15), 1924–1932.

Hiriart-Urruty, J.-B., Lemaréchal, C., 2001. Fundamentals of Convex Analysis. Springer Berlin Heidelberg.

Klarbring, A., Barber, J., Spagnoli, A., Terzano, M., 2017. Shakedown of discrete systems involving plasticity and friction. European Journal of Mechanics-A/Solids 64, 160–164.

Koiter, W., 1960. General problems for elastic solids. Progress in solid mechanics.

Mahtabi, M. J., Shamsaei, N., 2016. A modified energy-based approach for fatigue life prediction of superelastic niti in presence of tensile mean strain and stress. International Journal of Mechanical Sciences 117, 321–333.

Matoušek, J., Sharir, M., Welzl, E., 1992. A subexponential bound for linear programming. In: Proceedings of the eighth annual symposium on Computational geometry. pp. 1–8.

Melan, E., 1936. Theorie statisch unbestimmter systeme aus ideal-plastischen baustoff. Sitz.Berl.Ak.Wiss. 145, 195–218.

Nguyen, Q., 2003. On shakedown analysis in hardening plasticity. J.Mech.Phys.Solids 51, 101–125.

Peigney, M., 2006. A time-integration scheme for thermomechanical evolutions of shape-memory alloys. C.R.Mécanique 334, 266–271.

Peigney, M., 2009. A non-convex lower bound on the effective free energy of polycrystalline shape memory alloys. J.Mech.Phys.Solids 57, 970–986.

Peigney, M., 2010. Shakedown theorems and asymptotic behaviour of solids in nonsmooth mechanics. Eur.J.Mech. A.Solids 29, 784–793.

Peigney, M., 2013a. On the energy-minimizing strains in martensitic microstructures-part 1: Geometrically nonlinear theory. J.Mech.Phys.Solids 61, 1489–1510.

Peigney, M., 2013b. On the energy-minimizing strains in martensitic microstructures-part 2: Geometrically linear theory. J.Mech.Phys.Solids 61, 1511–1530.

Peigney, M., 2014a. On shakedown of shape memory alloys structures. Annals of Solid and Structural Mechanics 6 (1-2), 17–28.

Peigney, M., 2014b. Shakedown of elastic-perfectly plastic materials with temperature-dependent elastic moduli. Journal of the Mechanics and Physics of Solids 71, 112–131.

Peigney, M., 2018. Cyclic steady states in diffusion-induced plasticity with applications to lithium-ion batteries. Journal of the Mechanics and Physics of Solids 111, 530–556.

Peigney, M., 2020. Static and kinematic shakedown theorems in diffusion-induced plasticity. Journal of Theoretical and Applied Mechanics 58.

Peigney, M., 2023. A micromechanically consistent energy estimate for polycrystalline shape-memory alloys. i-general formulation. Journal of the Mechanics and Physics of Solids 172, 105165.

Peigney, M., Scalet, G., Auricchio, F., 2018. A time integration algorithm for a 3d constitutive model for smas including permanent inelasticity and degradation effects. International Journal for Numerical Methods in Engineering 115 (9), 1053–1082.

Peigney, M., Seguin, J., 2013. An incremental variational approach to coupled thermo-mechanical problems in anelastic solids. application to shape-memory alloys. Int. J. Sol. Struct. 50 (24), 4043–4054.

Peigney, M., Seguin, J., Hervé-Luanco, E., 2011. Numerical simulation of shape memory alloys structures using interior-point methods. Int. J. Sol. Struct. 48 (20), 2791–2799.

Pelton, A., Schroeder, V., Mitchell, M., Gong, X.-Y., Barney, M., Robertson, S., 2008. Fatigue and durability of nitinol stents. Journal of the mechanical behavior of biomedical materials 1 (2), 153–164.

Pham, D., 2008. On shakedown theory for elastic-plastic materials and extensions. J.Mech.Phys.Solids 56, 1905–1915.

Pham, D. C., 2017. Consistent limited kinematic hardening plasticity theory and path-independent shakedown theorems. International Journal of Mechanical Sciences 130, 11–18.

Raniecki, B., Mroz, Z., 2008. Yield or martensitic phase transformation conditions and dissipation functions for isotropic, pressure-insensitive alloys exhibiting sd effect. Acta mechanica 195 (1-4), 81–102.

Rankine, W. J. M., 1843. On the causes of the unexpected breakage of the journals of railway axles; and on the means of preventing such accidents by observing the law of continuity in their construction. In: Minutes of the Proceedings of the Institution of Civil Engineers. Vol. 2. Thomas Telford-ICE Virtual Library, pp. 105–107.

Scalet, G., 2018. An efficient algorithm for the solution of min-max problems in multiaxial fatigue. International Journal of Fatigue 112, 117–129.

Scalet, G., Karakalas, A., Xu, L., Lagoudas, D., 2021. Finite strain constitutive modelling of shape memory alloys considering partial phase transformation with transformation-induced plasticity. Shape Memory and Superelasticity 7 (2), 206–221.

Scalet, G., Peigney, M., 2017. A robust and efficient radial return algorithm based on incremental energy minimization for the 3d souza-auricchio model for shape memory alloys. European Journal of Mechanics-A/Solids 61, 364–382.

Shaw, J. A., Kyriakides, S., 1995. Thermomechanical aspects of niti. Journal of the Mechanics and Physics of Solids 43 (8), 1243–1281.

Silva, M., Shepherd, E. F., Jackson, W. O., Dorey, F. J., Schmalzried, T. P., 2002. Average patient walking activity approaches 2 million cycles per year: pedometers under-record walking activity. The Journal of arthroplasty 17 (6), 693–697.

Souza, A., Mamiya, E., Zouain, N., 1998. Three-dimensional model for solids undergoing stress-induced phase transformations. Eur.J.Mech. A 17, 789–806.

Waimann, J., Junker, P., Hackl, K., 2017. Modeling the cyclic behavior of shape memory alloys. Shape Memory and Superelasticity 3, 124–138.

Wang, J., Moumni, Z., Zhang, W., 2017. A thermomechanically coupled finite-strain constitutive model for cyclic pseudoelasticity of polycrystalline shape memory alloys. International Journal of Plasticity 97, 194–221.

Welzl, E., 2005. Smallest enclosing disks (balls and ellipsoids). In: New Results and New Trends in Computer Science: Graz, Austria, June 20–21, 1991 Proceedings. Springer, pp. 359–370.

Wohler, A., 1858. Versuche uber biegung und verdrehung von eisenbahn-achscn wahrent der fahrt. Z. Bauwesen 8, 641.

Woodworth, L. A., Kaliske, M., 2022. A temperature dependent constitutive model for functional fatigue in shape memory alloys. Mechanics of Materials 165, 104126.

Xu, L., Baxevanis, T., Lagoudas, D., 2019. A three-dimensional constitutive model for the martensitic transformation in polycrystalline shape memory alloys under large deformation. Smart Materials and Structures 28 (7), 074004.

Yang, Q., Stainier, L., Ortiz, M., 2006. A variational formulation of the coupled thermo-mechanical boundary-value problem for general dissipative solids. Journal of the Mechanics and Physics of Solids 54 (2), 401–424.

Yu, C., Kang, G., Song, D., Kan, Q., 2012. Micromechanical constitutive model considering plasticity for super-elastic niti shape memory alloy. Comp.Mater.Sci. 56, 1–5.